Molecular compositions and optical properties of dissolved brown carbon in biomass burning, coal combustion, vehicle emission aerosols~~in smoke particles~~ illuminated by excitation-emission matrix spectroscopy and ~~Fourier transform ion cyclotron resonance mass spectrometry (~~FT-ICR MS~~)~~ analysis

Jiao Tang[1,4], Jun Li[*, 1], Tao Su[1,4], Yong Han[2], Yangzhi Mo[1], Hongxing, Jiang[1,4], Min Cui[2], Bin Jiang[1], Yingjun Chen[2], Jianhui Tang[3], Jianzhong Song[1], Ping'an Peng[1], Gan Zhang[*, 1]

[1]State Key Laboratory of Organic Geochemistry, Guangzhou Institute of Geochemistry, Chinese Academy of Sciences, Guangzhou 510640, China

[2]Department of Environmental Science and Engineering, Fudan University, Shanghai 200092, P.R. China

[3]Key Laboratory of Coastal Environmental Processes and Ecological Remediation, Yantai Institute of Coastal Zone Research, Chinese Academy of Sciences, Yantai 264003, China

[4]University of Chinese Academy of Sciences, Beijing 100049, China

***Corresponding authors:** Jun Li (junli@gig.ac.cn); Gan Zhang (zhanggan@gig.ac.cn)

Abstract: Brown carbon (BrC) plays an essential impact on radiative forcing due to its ability to absorb sunlight. In this study, ~~We investigated~~ the optical properties and molecular characteristics~~fluorescence and chemical structural characteristics~~ of water-soluble and methanol-soluble organic carbon (MSOC)~~dissolved brown carbon (BrC) in smoke particulates~~ emitted from the combustion of biomass and fossil fuels and vehicle emissions ~~(coal and vehicle exhaust)~~ were investigated ~~–~~by UV-visible spectroscopy, excitation-emission matrix (EEM) spectroscopy and Fourier-transform ion cyclotron resonance mass spectrometry (FT-ICR MS) coupled with electrospray ionization (ESI). The results showed that these smoke aerosols of biomass burning (BB) and coal combustion (CC) had a higher mass absorption efficiency at 365 nm (MAE_{365}) than that of vehicle emissions. A stronger MAE_{365} value was also found in MSOC than water-soluble organic carbon (WSOC), indicating low polar compounds would possess higher light absorption capacity. Parallel factor analysis (PARAFAC) identified six types of fluorophores in the WSOC including two humic-like substances (HULIS-1) (P1, and P6), three protein-like substances (PLOM) (P2, P3, and P5), and one undefinition (P4). HULIS-1 was mainly from aging vehicle exhausts, P2 was only abundant in BB aerosols, P3 was ubiquitous in all tested aerosols, P4 was abundant in fossil burning aerosols, and P5 was more intense in the fresh vehicle-exhaust particles. The MSOC chromophores (six components, C1-C6) exhibited consistent characteristic with WSOC, suggesting the method could be used to indicate the origins of chromophores. FI-ICR mass spectra showed that CHO and CHON were the most abundant components of WSOC, but S-containing compounds appeared a higher abundance in the CC aerosols and vehicle emission than BB aerosols. While considerably low S-containing compounds with largely CHO and CHON were detected in MSOC. The unique formulas of different sources determined by the Venn diagram presented different molecular distribution. To be specific, BB aerosols with largely CHO and CHON had a medium H/C and low O/C ratio; while, CC aerosols and vehicle emission with largely S-containing compounds had an opposite H/C and O/C ratio. Moreover, the light absorption capacity of WSOC and MSOC was positively associated with the unsaturation degree and molecular weight in the source

设置了格式: 字体: Times New Roman

设置了格式: 字体: Times New Roman

设置了格式: 下标

设置了格式: 下标

aerosols. The above results are potentially applicable to further studies on EEM-based or molecular characteristic-based source apportionment of chromophores in atmospheric aerosols.

~~Six components were resolved by parallel factor analysis (PARAFAC) of the water-soluble and methanol-soluble organic carbon (MSOC) fractions, respectively. These fluorescent components varied among sources. Combined with FT-ICR MS ion groups, we found that the fluorescent components agreed well with the functional groups, particularly with nitrogen (N)- and sulfur (S)-containing groups. Among the six PARAFAC components (P1–6) retrieved from the water-soluble organic carbon (WSOC) fraction, except for the P3 component, the other components exhibited different values among the three types of emission sources tested. Vehicle exhaust was characterized by high P1 and P6 components, which are mainly associated with aromatic organosulfate compounds, and a high P5 component, mainly associated with sulfonates; coal combustion was characterized by a high P4 component, which is associated with nitrooxy-organosulfate (nitrooxy-OS) compounds; and biomass burning was characterized by the P2 component. Similar results were observed in the case of the MSOC fraction. This study reveals the source contribution and possible structures of previously unclear excitation-emission matrix (EEM) fluorescent components in combustion-derived aerosols. These are the first findings of this type and are potentially applicable to further studies on EEM-based source apportionment of dissolved BrC in aerosols.~~

1 Introduction

Carbonaceous aerosols play an important role in the Earth's radiative balance. One such aerosol, black carbon (BC), absorbs significant amounts of light and exerts a warming effect, while organic carbon (OC) was initially thought to only scatter solar radiation (Wong et al., 2017;Mo et al., 2017;Saleh et al., 2014). However, recent studies show that there are certain types of OC that absorb radiation efficiently in the near ultraviolet (UV) (300–400 nm) and ~~UV-~~visible ~~(UV-Vis)~~ ranges, which are called brown carbon (BrC). They can~~and are~~ able to positively shift the net direct radiation forcing (DRF) (Saleh et al., 2014;Laskin et al., 2015;Kirchstetter and Thatcher, 2012). According to a simulation model, the inclusion of BrC may enhance total aerosol absorption by 7–19% (Feng et al., 2013). According to previous study, BrC in atmospheric aerosols mainly originates from emissions from biomass burning (BB) and ~~fossil fuel combustion,~~coal combustion (CC)~~-~~, vehicle exhausts, and the formation of secondary organic aerosol (SOA) (Zhu et al., 2018;Laskin et al., 2015 Xie et al., 2017;Kumar et al., 2018). Among ~~the various sources listed above~~them, primary emissions contributed significantly to BrC absorption (Fan et al., 2012;Yan et al., 2015;Zhang et al., 2011). Recently, many studies have investigated the optical properties and molecular characteristic of BrC in laboratory simulated combustion (Budisulistiorini et al., 2017;Lin et al., 2018;Lin et al., 2016;Song et al., 2019)~~chemical and optical properties of BrC in smoke particles emitted from biomass burning, coal combustion in a control laboratory chamber~~ and their light absorption in controlled~~emissions characteristic of~~ vehicle emissions (Xie et al., 2017)~~-~~. However, there were no available studies on the comprehensive characteristic of BrC in various sources and their variations in optical and chemical information impacted by these sources, therefore, investigating the BrC in different sources would improve our understanding of the evolution of BrC absorption.

~~However, most studies mainly focused on light absorption of BrC; little structural information is available.~~

Excitation-emission matrix (EEM) spectroscopy can provide structure information of chromophores, and thus has been widely applied to identify the sources and chemical

设置了格式: 字体: Times New Roman

设置了格式: 字体: Times New Roman

设置了格式: 字体: Times New Roman

设置了格式: 字体: Times New Roman

域代码已更改

设置了格式: 字体: Times New Roman

设置了格式: 字体: Times New Roman

nature of chromophoric dissolved organic matter (CDOM) in aquatic environments since the 1990s (Shimabuku et al., 2017;Wells et al., 2017;Bhattacharya and Osburn, 2017;Coble, 1996), ~~while few studies have focused on the fluorescence properties of chromophores in atmospheric environments. Recently, many studies have suggested that the~~Due to the optical properties of chromophoric water-soluble organic carbon (WSOC) in the atmosphere ~~was~~ were similar to CDOM in aquatic environments (Qin et al., 2018;Fu et al., 2015;Graber and Rudich, 2006), ~~and~~ this technique could ~~be~~ extend~~ed~~ to atmospheric research. It has to be mentioned that ~~Fluorescence~~ fluorescence is a radiative process that occurs between two energy levels of the same multiplicity (Andrade-Eiroa et al., 2013). Generally, ~~C~~compounds with rigid planar structures and highly conjugated systems have intrinsic fluorescence emission characteristics and are important BrC chromophores, such as aromatic acids, phenols, nitroaromatics, polycyclic aromatic hydrocarbons (PAHs), quinones, and so on~~, which are important BrC chromophores~~ (Lin et al., 2018;Zhang et al., 2013)~~. Furthermore, Laskin et al. believed that fluorescence is sensitive to the molecular (or supramolecular) identity of BrC compounds and anticipated that fluorescence based methods will become increasingly important in the study of BrC~~. Therefore, chromophores in ~~Fluorescence~~ fluorescence spectra~~, which are~~ could be considered a "fingerprinting" tool, especially when combining it with parallel factor (PARAFAC) analysis which can decompose EEMs signal into their underlying chemical components (Murphy et al., 2013)~~have been applied to organic aerosols . Chen et al.~~ For instance, ~~(~~Chen et al., (2016b) observed that the ~~fluorescence spectra of~~ water-~~soluble~~ extracted ~~organic matter~~chromophores identified by PARAFAC from the urban, forest, and marine aerosols were varied ~~depending on~~with the sampling site~~s~~ and period~~s~~, and were affected by oxidative and functional groups. ~~Lee et al.(~~Lee et al., (2013) ~~reported~~ illustrated that SOA derived from the oxidation of limonene and decene with O_3 and OH had ~~presented~~ different fluorescence spectra. Therefore, BrC characteristics from various sources may differ. ~~The biggest challenge w~~When analyzing chromophoric BrC using fluorescence spectra, however, is the lack of a classification system for fluorescence spectra, to distinguish chromophores from ~~the~~

设置了格式: 字体: Times New Roman
设置了格式: 字体: Times New Roman
设置了格式: 字体: Times New Roman
设置了格式: 字体: Times New Roman
设置了格式: 字体: Times New Roman
设置了格式: 字体: Times New Roman
域代码已更改

~~majority of~~most non-absorbing constituents and to determine the chemical structures of the chromophores.

~~The combination of~~ Fourier-transform ion cyclotron resonance mass spectrometry (FT-ICR MS) coupled with electrospray ionization (ESI) ~~and EEM~~ is a powerful platform for the detailed characteristics investigation of organic material at the molecular level.~~characterizing BrC chromophores, and is expected to enable us to deduce the molecular compositions of these chromophores.~~ With the advantage of ultrahigh-resolution, the accuracy of mass measurements, and high sensitivity (Feng et al., 2016), FT-ICR MS has been successfully used to characterize organic aerosol (Jiang et al., 2016;Song et al., 2018;Mo et al., 2018), cloud water (Zhao et al., 2013), and natural organic matter (Sleighter et al., 2012;Feng et al., 2016). For example, a relative study determined their molecular families of dissolved organic matters (DOMs) associated with fluorescent components by using FI-ICR MS (Stubbins et al., 2014), which could provide more chemical information of chromophores. ~~The ultrahigh resolution, accuracy of mass measurements, and high sensitivity make this technique suitable for studying complex mixtures at the molecular level, and for identifying the chemical compositions of the substances being studied with a high degree of confidence (Feng et al., 2016).~~

Residential ~~coal combustion~~CC and ~~biomass burning~~BB emissions, and motor vehicle emissions are significant anthropogenic sources of air pollutants, exceptionally fine particulate matter ($PM_{2.5}$) on urban and regional scales (Gentner et al., 2017;Yan et al., 2015;Zhang et al., 2018;Chen et al., 2015). ~~are very important anthropogenic sources of air pollutants, especially fine particulate matter ($PM_{2.5}$), in China (Tian et al., 2017). Concerns about the environmental and health effects of vehicle emissions have existed for decades (Dai et al., 2015). The characteristics of BrC from these origins may differ to those of BrC from other sources.~~ In this study, ~~T~~to obtain a comprehensive understanding of BrC originating from different sources, UV-vis, EEMs, and FI-ICR MS analysis were performed for water-soluble and methanol-soluble organic carbon (MSOC) from the smoke particles of simulated combustion of biomass fuels and coals, and vehicle emission aerosols. Statistical

设置了格式：字体：Times New Roman

设置了格式：下标

analysis of PARAFAC was applied to EEM spectra to resolve the fluorescent compounds. All, and unique molecular characteristic of water-soluble organic carbon (WSOC) and MSOC were analyzed and discussed on the base of FI-ICR MS. Relationship between optical properties and chemical structures were discussed by using linear regression coefficient.~~we investigated the solvent extractions of organic compounds with different polarities from the smoke particles of simulated combustion emissions from biomass fuel, coal, and vehicles, and characterized their optical properties in terms of UV-Vis absorption and excitation-emission matrix (EEM) spectra. We employed FT-ICR MS coupled with ESI to investigate the molecular compositions of the fluorescent components identified by parallel factor analysis (PARAFAC). We also aimed to identify the possible chemical structures of these chromophores and create a source library of BrC chromophores for applications to atmospheric BrC apportionment based on fluorescence technology.~~

2 Experimental methods

2.1 Sample collection and preparation

The smoke particles were collected by the instrument coupled with dilution channel which was designed to simulate fire emissions representative of "real-world" open ~~biomass burning~~BB and household ~~coal combustion~~CC activities (Figure S1). In the present study, a total of 27 ~~biomass burning~~BB samples (IDs~~:~~ 1-27) were collected at Xishuangbanna city, Yunnan Provence, from May 20th to June 3th, 2016 and the detailed sampling process was described in our previous article (Cui et al., 2018). In short, raw fuels (rough 20×3×2 cm^3) were air-dried for several days, and ignited in a ~~stainless~~ stainless-steel bowl, and then the rising smoke was collected through a dilution system. The sampling system mainly consisted of a dilution tunnel, a residence time chamber, three particulate matter (PM) samplers, and so on. Every biomass was burned three times, about 1-2 kg fuels per burn. Every combustion process lasted for 20 minutes.~~Every biomass about 1-2 kg fuels was burned three times, and each combustion process lasted for 20 minutes.~~ The collection of smoke

particle started when fuel ignited, and end until the concentration of CO_2 down to atmosphere CO_2 level. Dilution ratios of each experimental process were calculated using the CO_2 concentrations before and after dilution. The collection flow rate and average dilution ratio were 180 L/min and 2.1, respectively. And the other 6 ~~biomass burning~~BB samples (IDs~~: –~~28-33) were collected at Guangzhou city, Guangdong Province.

The smoke particles of ~~coal combustion~~CC (IDs~~: -~~34-50) were collected as same as that of ~~biomass burning~~BB experiment, but used a stove, ~~at~~ in Guangzhou city, Guangdong province, from Nov ~~–~~18th, 2017 to Jan 23th, 2018. The tested stove is technically improved stoves (named Jin-Yin stove). Due to the difficult of ignition of coal, we used smokeless charcoal to ignite one-third (about 300 g) of the raw-coal chunk (2-5 cm in size) in the stove, removed the charcoal after ignition, and then added the remaining raw-coal chunk (about 700 g) to start to collect the smoke particle. Every coal was also burned three times, about 1 kg fuels per burn. Every combustion process lasted for about 40-150 minutes.~~Every coal about 1 kg fuels was burned three times, and each combustion process lasted for about 40-150 minutes.~~ The collection flow rate and average dilution ratio were 150 L/min and 1.5, respectively. Additionally, ~~a~~ modified combustion efficiency (MCE) was calculated to characterize the relative amount of smoldering and flaming combustion phase (Lin et al., 2016;Cui et al., 2018). The average MCE value~~s~~ were 0.73 ± 0.08 for ~~coal combustion~~CC experiment~~, –~~ but unavailable for the ~~biomass burning~~BB experiment because the CO sensor did not work in the field work which was mentioned in our previous paper (Cui et al., 2018).

Tunnel aerosols (total eight samples, IDs51-58) ~~Eight tunnel samples (IDs: 51-58)~~ were collected at Siping Tunnel from Nov 1th to 2th, 2017 and Xiaoyangshan Tunnel from Dec 1th to 2 th, 2017, in Shanghai city, as well as two vehicle exhaust particles (IDs59-60)~~two vehicle exhaust samples (IDs: 59-60)~~ were collected from the direct emission of two different trucks (more fresh aerosols). With no other instructions, vehicle emissions represented all tunnel aerosols and vehicle exhaust particles. The filters were wrapped in aluminum foil and pre-baked at 450 °C for 5 hours before

sampling~~,~~ and stored at -20 °C after sampling. Overall, ~~There~~ there were a total of 60 total suspended particulate matter (TSP) samples on source emissions in th~~e~~ ~~current~~is ~~experiment~~study, and blank samples ~~which~~ that were collected at different times and locations were used for correcting filter samples.

WSOC for UV-Vis absorption and EEM analysis was extracted with purified water (resistivity of >18.2Ω) via ultra-sonication of quartz filter punches for 30 minutes. Because water cannot effectively extract the BrC (Liu et al., 2013;Shetty et al., 2019), the remaining filter was further freeze-dried and extracted with methanol (HPLC grade) to~~After the extraction, we~~ obtain~~ed~~ the ~~methanol-soluble organic carbon (~~MSOC~~)~~ constituent for better understand the optical properties and molecular composition of BrC. ~~by freeze drying the water-extracted filter and performing ultrasonic-extraction with methanol (HPLC grade) in the same manner.~~ It is worth ~~Note~~ noting that the MSOC ~~fraction of the methanol extract~~ in ~~our current~~this study ~~are~~ is not necessarily ~~similar to~~like those of the same names in other studies. All the ~~of the~~ extracts were filtered through a 0.22 μ~~u~~m polytetrafluoroethylene membrane into amber colored glass vials to remove the insoluble material.

设置了格式: 字体: Times New Roman

2.2 Carbon analysis

We measured both OC and elemental carbon (EC) using an aerosol carbon analyzer (Sunset Laboratory, Inc., USA), following the NIOSH thermal-optical transmittance (TOT) standard method (Mo et al., 2017), and the emission factors (EFs) of PM, OC and EC were calculated and detail information was presented in supplement. We also analyzed the elemental compositions of biomass (C, H, O, and N) and coal (C, H, O, N, and S) using an elemental analyzer (vario EL cube; Elementar, Germany) and the results were listed in Table S1 and S2. The carbon content of WSOC were measured using total organic carbon analysis (Vario TOC cube; Elementar) before acidifying with phosphoric acid to remove inorganic carbon, while that of the MSOC ~~fractions were~~ was assessed using the method developed by ~~Chen et al.~~ a previous study (Chen et al., 2017b). In short, the extracted MSOC ~~fraction~~ was dried gently under nitrogen, and then re-dissolved in 500 μL methanol. Subsequently, 50 μL of the solution was

added to the clear quartz filter (area: 1.5 cm^2) until dry, and analyzed using the TOT standard method.

2.3 UV−Vis absorption spectra and EEM fluorescence spectra

The UV-vis absorption and ~~absorption and~~ EEM spectra of ~~the~~ WSOC and MSOC ~~samples~~ were analyzed using a UV-Vis spectrophotometer (UV-4802; Unico, China) and an Aqualog fluorometer (Horiba Scientific, USA), respectively. The wavelengths used to characterize the UV-~~Vis~~ vis spectra were between 200 to 800 nm at a step size of 2 nm. Purified water was used as a baseline correction before measure. Mass absorption efficiency (MAE, m^2 g^{-1} C) ~~can be~~was obtained as following equation (Li et al., 2018):

$$MAE_\lambda = A_\lambda \bullet \ln(10) / (C \bullet L) \quad (1)$$

Here, A_λ is the value of light absorption at given wavelength given by the spectrophotometer; C (μg C mL^{-1}) is the concentration of WSOC and MSOC ~~fractions~~; L is the optical path length. Moreover, the pH of WSOC ~~fraction~~ was measured for all samples within the range of 5.5-6.5, generally thought it ~~didn't~~ did not affect the absorbance according to prior study (Chen et al., 2016a).

The emission and excitation wavelengths of the fluorescence spectra were from 245 to 580 nm and 240 to 500 nm, respectively. The wavelength increments of the emission and excitation scans were 4.66 and 3 nm, respectively. Further, we subtracted the contributions of the solvents to the fluorescence spectra.

2.4 Ultrahigh resolution ESI FT-ICR MS analysis

The WSOC and MSOC of six selected samples including two BB aerosols (Musa and Hevea), two CC aerosols (a anthracite and bituminous coal), one day of tunnel aerosol (combined the aerosols in inlet and outlet of the tunnel in the same day, TA), and one vehicle exhaust particles were analyzed using FT-ICR MS. ~~Two fractions of six samples (IDs: 18 and 23 represented the mean fluorescence level of biomass burning; IDs: 38 and 46 represented anthracite and bituminous coal, respectively; IDs: 55 represents a day's worth of samples of tunnel inlet and outlet, and IDs: 59 represents~~

~~direct vehicle exhaust) were selected for FT-ICR MS analysis.~~ To remove inorganic ions ~~prior to~~before instrumental analysis, ~~the~~ WSOC ~~fraction~~ was further adjusted to pH = 2 by the addition of hydrochloric acid (HCl)~~,~~ and then passed through a solid-phase extraction cartridge (Oasis HLB, 30 um, 60 mg/cartridge; Waters Corporation, USA). The constituent retained on the SPE cartridge were eluted with methanol containing 2% ammonia (v/v). Eluted samples were evaporated until dry under a gentle nitrogen gas stream. The extracted solutions by methanol was ~~also~~ evaporated under a gentle nitrogen gas stream for preparation.

We used the analysis method of FT-ICR MS described in detail in ~~one of~~ our previous ~~studies~~ study (Mo et al., 2018). Briefly, ~~ultrahigh~~ ultrahigh-resolution mass spectra were obtained using a solariX XR FT-ICR MS (Bruker Daltonics GmbH, Bremen, Germany) equipped with a 9.4-T superconducting magnet and an ESI ion source. The system was operated in negative ionization mode. The ion accumulation time was set to 0.6 s. The lower and upper mass limit was set to m/z 150 and 800 Da, respectively. The mass spectra were externally calibrated with arginine clusters using a linear calibration and then internally recalibrated with typical O_6S_1 class species peaks using quadratic calibration in DataAnalysis ver. 4.4 software (Bruker Daltonics). A typical mass-resolving power >450 000 at m/z 319 with <0.2 ppm absolute mass error was achieved. The mass spectra of field blank filters were analyzed to detect possible contamination following the same procedures. More data processing was presented in S1 of supplement.

2.5 PARAFAC analysis for EEM spectra

~~Parallel factor (~~PARAFAC~~)~~ analysis with non-negativity constrains was used to explore the fluorescent components in dissolved BrC based on the method established by Murphy et al (Murphy et al., 2013;Andersson and Bro, 2000), which was performed using drEEM toolbox version 2.0 using a MATLAB software (http://models.life.ku.dk/drEEM). This method had been widely applied to the analysis of fluorescence spectra in aerosol (Chen et al., 2016b;Chen et al., 2016a;Matos et al., 2015;Wu et al., 2019). Absorbance measurements was used to

correct the EEMs for inner filter effects (IFE) according to the previous studies (Luciani et al., 2009;Gu and Kenny, 2009;Fu et al., 2015). The highest light absorbance in the calibrated wavelength range of WSOC and MSOC ~~in two fractions~~ was not greater than 2 (mostly below 1 at 254 nm), which is appropriate for the inner filter corrections of the EEMs (Gu and Kenny, 2009;Murphy et al., 2013). Each EEM was normalized to the Raman peak area of purified water collected on the same day to correct fluorescence in Raman Units (RU) at excitation 350 nm~~,~~ and corrected for the dilution factor (Murphy et al., 2013;Murphy et al., 2010). Additionally, the signals of the first-order and second-order Rayleigh and Raman scattering in the EEM were removed by ~~using~~ an interpolation method (Bahram et al., 2006). Repeated convergence of the model was examined based on the iteration of the minimum squares principle. The exploration phases of 2- to 7-componet PARAFAC models ~~were~~ contained that evaluation of the shape of spectral loading, leverage analysis, examination of the core consistency, residual analysis, and split half analysis (Figure S2-S7). ~~Finally, s~~Six component PARAFAC model was identified and successfully passed the split validation ~~analysis~~ with the split style of "$S_4C_6T_3$" for the WSOC and MSOC ~~fraction~~ in 60 samples, respectively.

设置了格式: 字体: Times New Roman

3 Results and discussions

3.1 Emission Characteristics and Optical Properties of Extracts.

The PM, OC, and EC emission factors (EFs) of 27 biomass and 17 coal combustion experiments ~~are~~ were summarized in Table S3. The relevant EFs of some of the biomass species were reported previously (Cui et al., 2018). In the ~~current~~is experiment, the EFs of PM, OC, and EC from burning 27 types of biomass were 15 ± 11 g kg^{-1} fuel, 8.0 ± 6.4 g kg^{-1} fuel, and 7.7 × 10^{-1} ± 3.4 × 10^{-1} g kg^{-1} fuel, respectively. The EFs emitted from bituminous ~~coal combustion~~CC (PM = 9.1 × 10^{-1} ± 6.5 × 10^{-1} g kg^{-1} fuel, OC = 4.2 × 10^{-1} ± 3.3 × 10^{-1} g kg^{-1} fuel, EC = 9.4 × 10^{-2} ± 1.9 × 10^{-1} g kg^{-1} fuel) were much higher than those of anthracite combustion (PM = 1.5 × 10^{-1} ± 8.9 × 10^{-2} g kg^{-1} fuel, OC = 1.2 × 10^{-2} ± 4.5 × 10^{-3} g kg^{-1} fuel, EC = 1.6 × 10^{-4} ± 1.4 × 10^{-4} g kg^{-1} fuel) in the same stove. These differences can be attributed to the high volatile

matter content of bituminous coal (Tian et al., 2017;Chen et al., 2005). Note that ~~coal smoke was collected~~ when the fire had been ignited using ~~one~~ one-third of the material, and then ~~after which~~ the remaining part was added, the CC smoke was collected. ~~.~~ Thus, the results of our study ~~were~~would be ~~.~~ lower than the real values.

~~Mass absorption efficiency (~~MAE~~)~~ can be used to characterize the efficiency of solar energy absorption, which is represented by the degree of conjugation and the amount of electron delocalization in molecules (Chen et al., 2016a). As shown in Figures ~~2b~~ 1~~and S8b,~~ and ~~in~~ Table S4, MAE at 365 nm (MAE_{365}) ~~is~~ was significantly higher in the case of BB and CC aerosols~~biomass burning and coal combustion~~ than in vehicle emissions in th~~e current~~is study~~.~~, consistent with the previous findings (Xie et al., 2017;Fan et al., 2016). Bituminous CC aerosols had higher MAE_{365} values than anthracite combustion aerosols. At there, we introduced the EC/OC ratios, which could be used as an indicator of fire conditions (Xie et al., 2017). Figure S8 showed the MAE365 of WSOC vs. EC/OC relationships for all BB and CC aerosols. The data clearly showed that the light absorption of BB aerosols was dependent on the burn conditions. However, weak relationship ($p>0.05$) in CC aerosols suggested another factor may influence the light absorption, such as maturity (Li et al., 2018). Compared to WSOC, ~~Higher~~ higher MAE_{365} values were observed in the MSOC ~~fractions~~ collected from ~~biomass burning~~BB (2.3 ± 1.1 m^2 $g^{-1}C$) and bituminous ~~coal combustion~~CC (3.2 ± 1.1 m^2 $g^{-1}C$) aerosols. ~~compared to their WSOC fraction values.~~ This ~~may~~ could be due to the fact that these strongly light-absorbing fat-soluble components are likely to be large molecular weight PAHs, and quinones from ~~biomass burning~~BB and fossil fuel combustion (Sun et al., 2007;Chen and Bond, 2010), which were more soluble in low polar solution, ~~while~~ but we obtained the opposite results in the case of anthracite combustion and vehicle emissions. ~~Moreover, the higher MAE_{365} in biomass burning and bituminous coal combustion represented a stronger absorbing ability in the case of the MSOC fraction, which reflected greater variation in the chemical composition than in the WSOC fraction.~~

The MAE_{365} of ~~biomass burning~~WSOC in this study was compared with the other studies (Figure 1). The BB aerosols in this study had a higher MAE_{365} value

设置了格式：下标

设置了格式：下标

than those in controlled BB experiments, while it was comparable to corn straw burning emissions (Park and Yu, 2016;Fan et al., 2016). Besides, the simulated BB aerosols exhibited higher MAE365 values than those in highly BB-impacted areas (Hecobian et al., 2010), indicating the aging in the transport process could reduce the light absorption (Dasari et al., 2019). The CC aerosols showed a higher MAE_{365} value than the other coal experiment (Li et al., 2018;Fan et al., 2016), while a comparable value to water-soluble BrC was observed in winter of Beijing (Cheng et al., 2011;Yan et al., 2015). The result indicated the strong influence of BrC in this season in this region. Besides, the simulated combustion aerosols in this study exhibited higher MAE_{365} values than the other areas (such as Guangzhou, Nanjing, Los Angeles, Korea, Nepal, and so on) (see Figure 1).

Methanol has a lower polarity than water and can extract the water-insoluble compounds that are generally stronger chromophores. Chen et al., (2017b) extracted organic matters in aerosols using different polar solutions, and they found water-insoluble organic matters (WIOM) had a higher MAE value than the water-soluble organic matters (WSOM), consistent with our result in the BB and bituminous CC aerosols. Vehicle emission aerosols generally had a lower MAE value such as methanol-soluble BrC (0.62 ± 0.76 m^2 $g^{-1}C$) in controlled emission experiment (Xie et al., 2017), which was comparable to WSOC (0.71 ± 0.30 m^2 $g^{-1}C$) but higher than MSOC (0.26 ± 0.09 m^2 $g^{-1}C$) in this study.

设置了格式：下标

设置了格式：下标

设置了格式：上标

设置了格式：上标

设置了格式：上标

设置了格式：上标

设置了格式：上标

设置了格式：上标

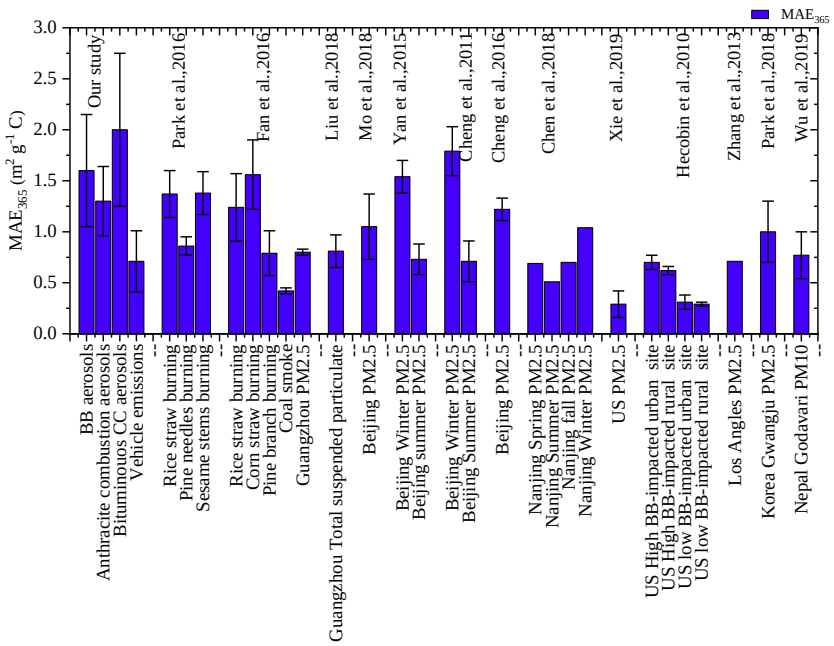

~~and coal combustion in the WSOC fraction was also higher than that of ambient aerosol and biomass and coal combustion experiments in a laboratory sampling system (Chen et al., 2018;Zhu et al., 2018;Yan et al., 2015;Li et al., 2018;Park and Yu, 2016) (Figure S4).~~ Figure 1, Comparison of MAE_{365} in the WSOC fraction of source emission aerosols with the other studies. The references were as following:(Liu et al., 2018;Mo et al., 2018;Yan et al., 2015;Cheng et al., 2011;Cheng et al., 2016;Xie et al., 2019;Hecobian et al., 2010;Zhang et al., 2013;Park et al., 2018;Wu et al., 2019;Fan et al., 2016;Park and Yu, 2016;Chen et al., 2018)

3.2 EEM spectra of WSOC and MSOC.~~dissolved BrC.~~

Fluorescence spectra was used to characterize the organic chromophores of different sources. We applied the PARAFAC model (Murphy et al., 2013) to determine the underlying chromophore components of the 60 emission source samples. Six typically independent components ~~of~~ in the WSOC ~~fraction~~ were resolved, as shown in the top of Figure ~~1~~ 2 and Table 1. Compared with the previous studies, the fluorescence~~EEM~~ of P1 and P6 were similar to those for 7CM-C1 (the C1 component of a seven-component model) and 7CM-C3, named humic-like substances

带格式的：缩进：首行缩进： 0 字符

设置了格式：字体：五号，加粗

设置了格式：字体：五号，加粗

设置了格式：字体：五号，加粗

设置了格式：字体：五号

设置了格式：字体：五号，下标

设置了格式：字体：五号

(HULIS-1)~~pertaining to water-extracted matter in urban and forest area, and marine aerosols, in Japan~~ (Chen et al., 2016b). Further, there were peaks in the emission wavelengths (> 400 nm) of P1 and P6, which were probably derived from conjugated systems (Chen et al., 2016b). The peak of the P3 component was almost located in region IV, which was categorized as a protein-like (cytidine) or tryptophan-like ~~(peak T)~~ fluorophore (Qin et al., 2018;Fan et al., 2016). Generally, peaks at shorter excitation wavelengths (< 250 nm) and shorter emission wavelengths (< 350 nm) are correlated with simple aromatic proteins such as tyrosine (Cory and Mcknight, 2005), which is ~~quite~~ similar to the ~~peak~~ fluorescence of ~~the~~ P2 component observed in this study. ~~According to a prior report, the spectra of the~~ P5 component was ~~also~~ similar to tryptophan- and tyrosine-like components (Chen et al., 2017a). Therefore, P2, P3, and P5 components were named protein-like substances (PLOM). ~~The spectra of the~~ P4 component ~~has been~~was reported relatively rarely but ~~is~~ similar to previously observed peaks that ~~are~~ were considered to arise mainly in surface water and algal secretions (Yu et al., 2015). It is worth noting ~~Note~~ that the origins and chemical structures of the chromophores studied are not necessarily ~~similar to~~like those of chromophores with the same names in other types of organic matter.

Table 1. The maximum excitation and emission wavelengths of the PARAFAC components from the WSOC and MSOC fractions extracted from the three origins

	PARAFAC component	Excitation maxima (nm)	Emission maxima (nm)	Assignment according to published papers	References
WSOC	P1	251, 314	415	HULIS-1, terrestrial humic-like component	(Chen et al., 2016b;Sgroi et al., 2017;Fu et al., 2015)
	P2	254	337	Tyrosine-like	(Cory and Mcknight, 2005)
	P3	287	360	Protein-like (cytidine) or tryptophan-like	(Qin et al., 2018;Fan et al., 2016)
	P4	251	374	-	-
	P5	278	319	Protein-like fluorophores	(Fu et al., 2015)

	P6	254, 371	485	HULIS-1, conjugated systems, a terrestrial humic or fulvic acid-like component	(Chen et al., 2016b)
MSOC	C1	308	356	-	
	C2	<250,272	388		
	C3	<250	434	C2 for the urban ASOM samples	(Matos et al., 2015)
	C4	257	360		
	C5	284	328		
	C6	269	310		

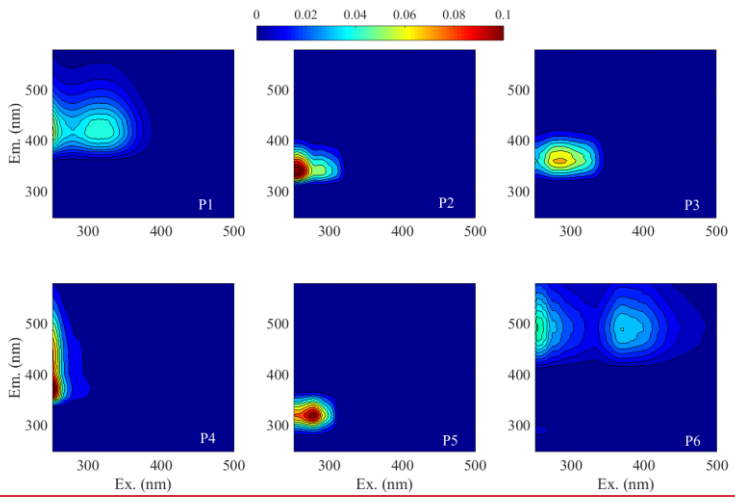

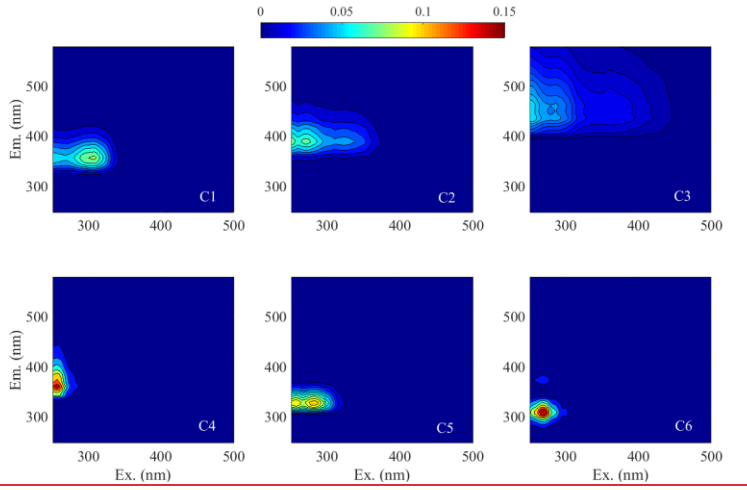
0
0.05
0.1
0.15
Em. (nm)
Ex. (nm)
C1
C2
C3
C4
C5
C6

421

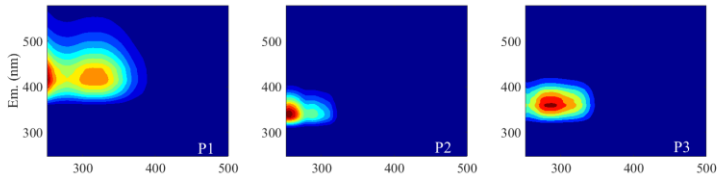
Em. (nm)
P1
P2
P3

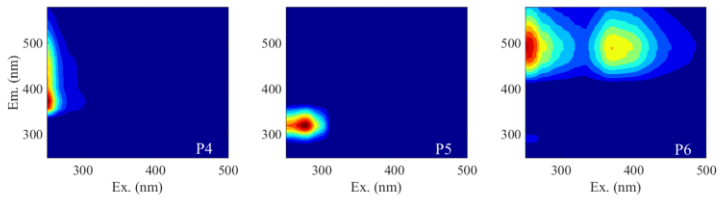
Em. (nm)
Ex. (nm)
P4
P5
P6

422

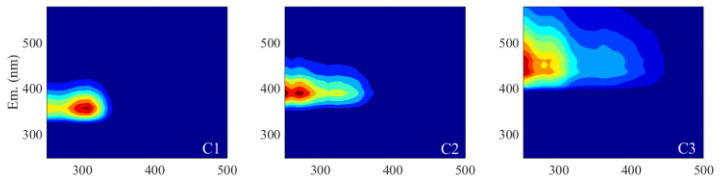
Em. (nm)
C1
C2
C3

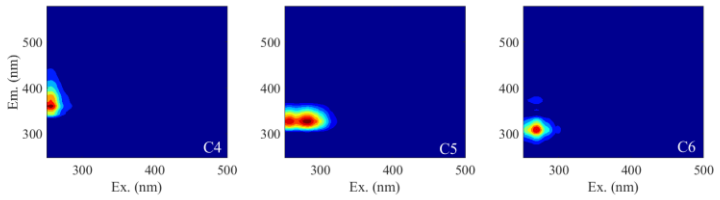
Em. (nm)
Ex. (nm)
C4
C5
C6

423

Figure ~~1~~2. The ~~excitation-emission matrix (~~EEM~~)~~ components ~~spectra determin~~identifie~~d~~ by ~~parallel factor (~~PARAFAC~~) analysis~~ of WSOC (top: P1-P6) and MSOC (bottom: C1-C6) extracted from three origins.

The results from the six-component model (abbreviated C1–6) of ~~the~~ MSOC ~~fractions~~ ~~–~~identified by PARAFAC, as described in the bottom of Table 1 and Figure ~~1~~2, were ~~obviously~~ different ~~to~~ from those ~~obtained~~ observed in~~for~~ the WSOC ~~fraction~~, indicating different chemical structures. The peak of C1 component was similar to that of the P3 component of ~~the~~ WSOC ~~fraction~~, but the excitation wavelength was higher than that of P3 component~~—~~. The higher excitation wavelength~~which~~ indicated the presence of conjugated unsaturated bond systems shifting towards the high wavelengths of ~~the~~ C1 component (Matos et al., 2015). Moreover, as reported ~~in a previous study~~, ~~the~~ C3 component was similar to ~~the~~ component ~~C~~2 ~~component~~ of urban alkaline-soluble organic matter (ASOM) ~~samples~~ collected from the city of Aveiro, Portugal (Matos et al., 2015). ~~Because the fluorescence spectrum of the MSOC fraction was poorly characterized, the molecular composition of the other fluorescent components was studied using FT-ICR MS.~~

The maximum fluorescence intensities (F_{max}) ~~(Table S5, S6) is~~ was calculated by multiplying the maximum excitation loading and maximum emission loading for each component by its score (Murphy et al., 2013). Generally, changes in the relative abundance of a component ($F_{max}/\sum F_{max}$) could indicate changes in its overall importance, which had been successful applied to study the origins of chromophores (Yan and Kim, 2017;Chen et al., 2017a;Chen et al., 2016b;Wu et al., 2019). In th~~e current~~is study, the relative abundances ~~intensities~~ of ~~different~~ fluorescent components in different types of samples was highly variable, depending on the sources (Figure 3a). ~~As shown in Figure 2a,~~ P1 component ~~was intense in the case of vehicle emission, accounting~~ accounted for an average of ~~30~~ 34 ± ~~84~~.37% of the total fluorescence intensities in the case of tunnel aerosols~~of vehicle emission.~~, which was higher than BB aerosols (mean ± SD: 19 ± 4.8%), CC aerosols (14 ± 3.8%) and vehicle exhaust particles (17 ± 1.0%). This result indicated P1 component had an aged vehicle exhaust origin because a difference of P1 component was observed from tunnel aerosols and

vehicle exhaust particles. In contrast, the fluorescence of P6 components was weak in any of the samples, but in vehicle emissions (9.4 ± 2.3%) was higher than BB and CC aerosols (both 2.5%). P5 component was more intense in the vehicle exhaust particles (30 ± 1.6%) than other sources. P2 ~~and P4~~ components ~~were~~ was only abundant in the cases of BB aerosols (33 ± 11%) but did not exhibit in vehicle emissions, suggested some structures responsible for this chromophore could not exist in vehicle emissions. ~~intense in the cases of biomass burning (mean: 33 ± 11% of fluorescence intensities of biomass burning) and~~ P4 component was the more abundant chromophore in CC aerosols (34% ± 7.7%) and vehicle emissions (29 ± 5.9%), especially in vehicle exhaust particles (38 ± 1.1%).~~coal combustion (mean: 34 ± 7.7%), respectively.~~ In contrast, P4 component in BB aerosols was weak (11% ± 7.9%), indicating a fossil origin. ~~The~~ P3 component~~s~~ ~~were~~ was almost equal across all samples. The possible reason ~~is~~ was that ~~the~~ P3 component~~s~~ ~~is~~ was similar to the peak of tryptophan-like compounds~~, where these are~~ which were common to practically all published models and are likely to be found in almost all sources (Yu et al., 2015). ~~It was obvious that P5 component was intense in direct vehicle exhaust (IDs: 59 and 60; mean: 30 ± 1.6%). In contrast, the fluorescence of P6 components was weak in any of the samples, but the P6 component in vehicle emissions (mean: 9.4 ± 2.2%) significantly exceeded those of biomass burning and coal combustion (both 2.5%). The above results clearly indicates that the chemical composition of chromophoric water-soluble BrC varies remarkably among sources.~~

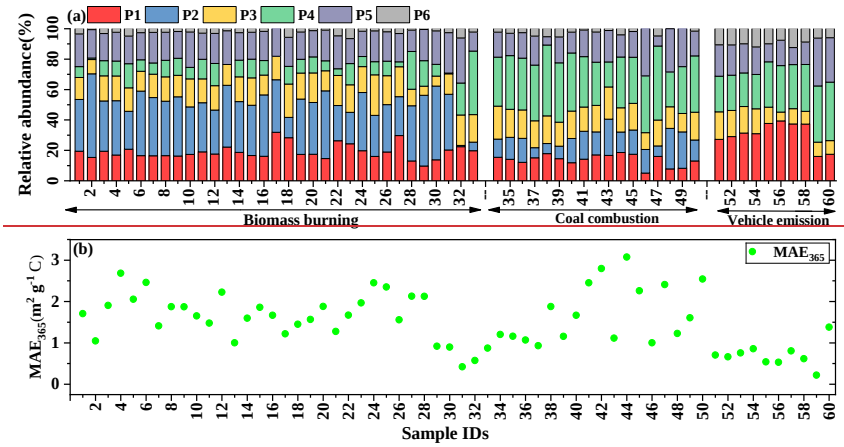

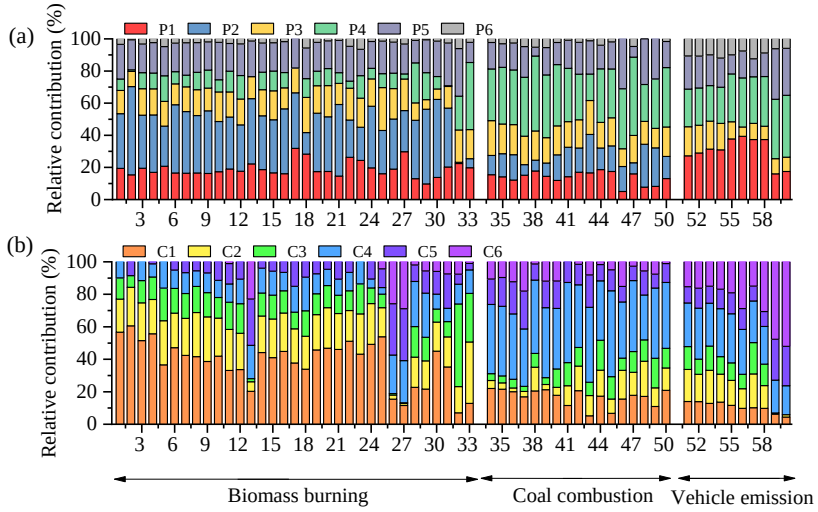

Figure ~~2~~3. The relative contribution of each PARAFAC component of WSOC (a) and MSOC (b) in the three source emissions. ~~(a) Relative abundance of each PARAFAC component, (b) mass absorption efficiency at 365 nm (MAE_{365}) values in WSOC fractions from three origins~~

The relative intensities of ~~the~~ fluorescent components in the MSOC ~~fraction~~ exhibited similar characteristics to the WSOC ~~fraction~~ (Figure ~~S8a~~3b). ~~The~~ C1 ~~and C2~~ component~~s~~ was the substances with more intense in the case of ~~biomass burning~~ BB aerosols (~~mean:~~ 38% ± 14 % ~~and 21 ± 6.9%, respectively~~) than the other sources. C2

component was enriched in BB aerosols (21% ± 6.9%) and tunnel aerosols (17% ± 6.9%) than those in CC aerosols and vehicle exhaust particles. Also, C2 exhibited a difference between bituminous CC and anthracite combustion aerosols, as well as tunnel aerosols and vehicle exhaust particles, indicating C2 component could be used to identify these sources. C4 component~~s~~ was intense in ~~samples of coal combustion~~CC aerosols (~~mean:~~ 41 ± 6.0%) and vehicle exhaust particles (25 ± 4.4%). ~~The levels of component~~ C3 component ~~were~~ was not ~~abundance~~ abundant among ~~between~~ the three sources and not observed in the vehicle exhaust particles, suggesting not a fresh vehicle-exhaust emission origin~~types of fuel tested~~. Instead of C3, ~~The~~ C5 and C6 components ~~was~~ were more intense in ~~direct~~vehicle exhaust particles ~~vehicular exhaust~~ (~~IDs: 59 and 60; mean:~~ 25 ± 6.8% and 50 ± 6.8%, respectively), suggesting they were more primary vehicle emission chromophores. ~~,~~ The last study observed that the relative abundances of various chromophores in aerosols with different particle sizes were different (Chen et al., 2019). Therefore, the fluorescence technique is sensitive for chromophores with different sources, sizes, and chemical structures and so on. Combining these results with the WSOC mentioned above results~~the above-mentioned WSOC results~~ and comparing the different characteristics and fuel source information, the fluorescent components obtained by EEM-PARAFAC ~~can~~ could potentially assist with the source apportionment of BrC for environmental ~~monitoring~~ applications.

3.3 Molecular composition detected by FT-ICR MS

~~**3.3 Molecular composition of FT-ICR MS and chemical structures of chromophores**~~

~~**The relative abundances of the four compound groups (CHO, CHON, CHOS, and CHONS) in the WSOC fraction are presented in Figure S9. These results were consistent with previous results (Song et al., 2018), in which S- containing compounds were mainly found in coal combustion emissions. Conversely, our results proved that N-containing substances were also abundant in coal**~~

设置了格式：字体：加粗

带格式的：左，定义网格后不调整右缩进，段落间距段前：7.8 磅，段后：7.8 磅，不调整西文与中文之间的空格，不调整中文和数字之间的空格

带格式的：段落间距段前：0 磅，段后：0 磅

设置了格式：字体：加粗

带格式的：左

设置了格式：字体：加粗

设置了格式：字体：加粗

~~combustion aerosols. One possible reason for this concerns the viable coal types; for example, significant differences were observed between water extracts of IDs 36 (anthracite coal) and 46 (bituminous coal). More detailed information about the molecular compositions is provided in Tables S7 and S8, and Figure S10, S11 and S12.~~

~~The previous study reported that potential BrC chromophores were identified by determining those compounds in the region between Double bond equivalent (DBE) = 0.5 × C and DBE = 0.9 × C (in the coordinate axis, the x-axis is the C number and the y-axis is the DBE value) (Lin et al., 2018). To explore the possible chemical structures of dissolved chromophores, the methods of the O/C and H/C ratios of matter or functional groups were used to classify the ion groups of FT-ICR MS as listed in Figure 2. Furthermore, according to the all ions or potential BrC ions, there are total four classifications. The first method is to follow their O/C and H/C ratios of matter to classify all ions of FT-ICR MS; the second method is to follow their O/C and H/C ratios of matter to classify potential BrC ions; the third method is to follow their functional groups to classify all ions; the last method is to follow their functional groups to classify potential BrC ions. The relationship between the relative intensities of classified group of ions (the ratio of intensities of each ion group to total ion intensities) and the relative abundance of fluorescent components were presented in Table S9-S16. The results indicated that the method that sorted the potential BrC ion groups by their functional groups is best for explaining the relationship between the chemical composition and fluorescent components. For example, the presence of L-CHON groups with O/N ≤ 2 suggests that these reduced N compounds may be associated with alkyl amides and alkyl nitrile, as well as heterocyclic aromatic compounds with single N atoms (Alexander et al., 2009;Song et al., 2018). The H-CHON group with O ≥ 3, O/N > 2 and AI$_{mod}$ > 0.5 suggests that these compounds contain O and N atoms, such as benzene rings substituted with O-containing groups (hydroxyl, and carboxyl) and nitro-aromatics (Chen et al., 2016b;Song et al., 2018;Lin et al., 2016). The H-CHOS group had O/S ≥ 4,~~

带格式的：左，首行缩进： 0 字符

设置了格式：字体：小四，加粗

设置了格式：字体：加粗

设置了格式：字体：加粗

设置了格式：字体：加粗

设置了格式：字体：加粗

设置了格式：字体：（默认）Times New Roman，加粗

设置了格式：字体：加粗

设置了格式：字体：加粗

设置了格式：字体：加粗

设置了格式：字体：加粗，非上标/ 下标

设置了格式：字体：加粗

设置了格式：字体：加粗

设置了格式：字体：加粗

~~suggesting the assignment of a sulfate group (OSO_3H). As sulfate groups carry four oxygen atoms and readily deprotonate in ESI, they are more likely to be organosulfates (Jiang et al., 2016). The presence of the H-CHONS group suggested not only the assignment of a sulfate group (OSO_3H), but also an additional one or two nitrooxy groups (ONO_2) (Mo et al., 2018).~~

设置了格式：字体：加粗，非上标/ 下标

设置了格式：字体：加粗

设置了格式：字体：加粗

设置了格式：字体：加粗

设置了格式：字体：加粗，非上标/ 下标

设置了格式：字体：加粗

设置了格式：字体：加粗，非上标/ 下标

设置了格式：字体：加粗

设置了格式：字体：加粗

设置了格式：字体：加粗

Table 2. The classification methods of ion groups of FT-ICR MS

Specific classification methods			
Function groups		H/C and O/C[a]	
CHO[1]	O[1]	Lipids	O/C=0–0.2, H/C=1.7–2.2
CHO[>1]	O[>1]	Proteins	O/C=0.2–0.6, H/C=1.5–2.2, N/C ≥ 0.05
L-CHON	O/N ≤ 2	H-Lignin	O/C = 0.1–0.6, H/C =0.6–1.7, 0.5 < AI$_{mod}$ < 0.67
H-CHON	O/N > 2	M-Lignin	O/C = 0.1–0.6, H/C =0.6–1.7, 0 < AI$_{mod}$ ≤ 0.5, DBE ≥ 4
L-CHOS	O/S < 4	L-Lignin	O/C = 0.1–0.6, H/C =0.6–1.7, 0 < AI$_{mod}$ ≤ 0.5, DBE < 4
H-CHOS	O/S ≥ 4	Carbohydrates	O/C = 0.6–1.2, H/C = 1.5–2.2
L-CHONS	O/S < 7(N[1]); O/S < 10 (N[2])	Tannins	O/C = 0.6–1.2, H/C = 0.5–1.5, AI$_{mod}$ < 0.67
H-CHONS	O/S ≥ 7(N[1]); O/S ≥ 10 (N[2])	Unsaturated hydrocarbons	O/C = 0–0.1, H/C = 0.7–1.5

Note that L, M, and H stands for low, moderate, and high, respectively; The lignin group is further divided into three subcategories on the base of their AI$_{mod}$ and DBE (H-Lignin: 0.5 < AI$_{mod}$ < 0.67; M-Lignin: 0 < AI$_{mod}$ ≤ 0.5, DBE ≥ 4; L-Lignin: 0 < AI$_{mod}$ ≤ 0.5, DBE < 4).

a: (Patriarca et al., 2018)

设置了格式：字体：小四
带格式的 ...
设置了格式：字体：小四，加粗
设置了格式：字体：小四
带格式的：左，行距：1.5 倍行距，无孤行控制
设置了格式：字体：小四
设置了格式 ...
带格式的：左，行距：1.5 倍行距，无孤行控制
设置了格式：字体：小四
带格式的：左，行距：1.5 倍行距，无孤行控制
设置了格式 ...
设置了格式 ...
设置了格式：字体：小四
带格式的：左，行距：1.5 倍行距，无孤行控制
设置了格式 ...
设置了格式 ...
设置了格式：字体：小四
带格式的：左，行距：1.5 倍行距，无孤行控制
设置了格式 ...
设置了格式 ...
设置了格式：字体：小四
带格式的：左，行距：1.5 倍行距，无孤行控制
设置了格式 ...
设置了格式 ...
设置了格式：字体：小四
带格式的：左，行距：1.5 倍行距，无孤行控制
设置了格式 ...
设置了格式：字体：小四
带格式的：左，行距：1.5 倍行距，无孤行控制
设置了格式 ...
设置了格式 ...
设置了格式：字体：小四
带格式的：左，行距：1.5 倍行距，无孤行控制
设置了格式 ...
设置了格式：字体：小四
带格式的：左
设置了格式 ...
设置了格式：字体：小四
带格式的：两端对齐，无孤行控制
设置了格式 ...

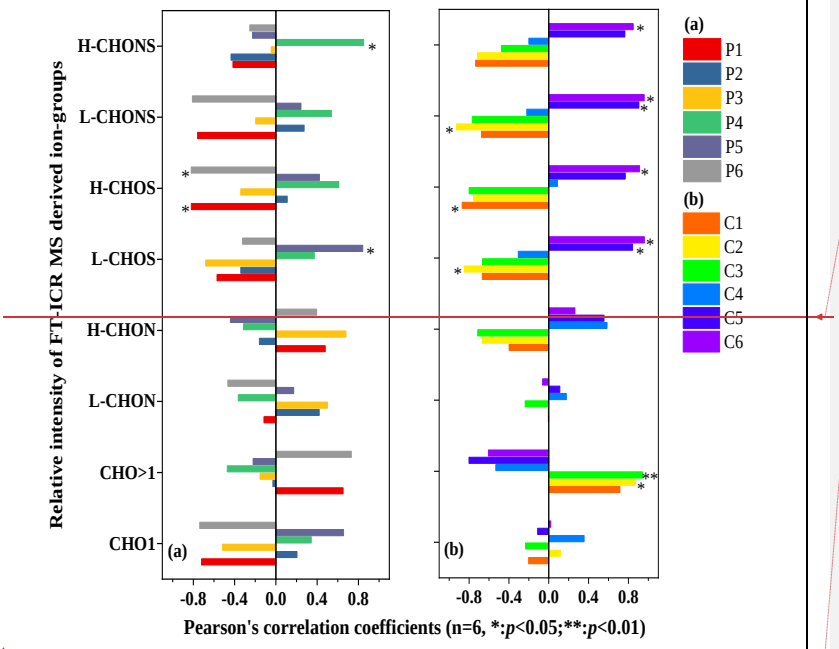

~~Figure 3. Pearson's correlation coefficients (r) and significance levels (two-sided t-test) obtained from the correlation analysis between the relative intensity of the ion groups based on Fourier-transform ion cyclotron resonance mass spectrometry (FT-ICR MS), and the relative intensity of the (a) six components of the WSOC fractions and (b) six components of the MSOC fractions.~~

~~3.3.1 Composition of chromophores of WSOC~~

~~The relationship between the relative intensities of the classified ion groups of FT-ICR MS and the relative contents of the PARAFAC components in the WSOC fraction were presented in Figure 3a and Table S15. The P1 and P6 components were both negatively correlated with the H-CHOS group ($p < 0.05$). Considering that P1 and P6 components was intense in samples of vehicle emissions, the main compounds detected from this source were O_4S_1–$O_{12}S_1$ class species with a wide range of C numbers (7–34) and double bonds equivalent (DBE) values (4–20), of which O_4S_1~~

设置了格式：字体：小四

设置了格式：字体：Times New Roman，小四

带格式的：首行缩进：0 字符

设置了格式：字体：Times New Roman，小四

设置了格式：字体：小四，非加粗

设置了格式：字体：Times New Roman，小四

设置了格式：字体：小四

设置了格式：字体：Times New Roman，小四

设置了格式：字体：小四

设置了格式：字体：非加粗

带格式的：段落间距段前：0 磅，段后：0 磅

设置了格式：字体：非倾斜

设置了格式

设置了格式：字体颜色：自动设置

设置了格式：字体颜色：自动设置

设置了格式：字体颜色：自动设置

设置了格式：非上标/ 下标

设置了格式：非上标/ 下标

设置了格式：非上标/ 下标

设置了格式：非上标/ 下标

设置了格式：非上标/ 下标

设置了格式：非上标/ 下标

and O_5S_1 class species, which exhibit an R-OSO_3H structure, were the most abundant. Among these chemical formulas, we found that many aromatic organosulfate isomers with relatively high DBE values ($\geq$ 4) were side chains or aromatic rings, and thus their chemical formulas could be those of alkylbenzene rings substituted with one sulfate and one hydroxyl group (Song et al., 2018), such as $C_8H_{10}O_5S$ (DBE: 4) and $C_{10}H_{10}O_6S$ (6). These structures were detected in humic-like substances (HULIS) from coal smoke and SOA generated under all experimental conditions (Riva et al., 2015;Song et al., 2018) and were likely responsible for the P1 and P6 components.

The P4 component was positively correlated with the H-CHONS group ($p < 0.05$), suggesting nitrooxy organosulfates (nitrooxy-OS) (Mo et al., 2018). Nitrooxy-OS is probably be formed by photooxidation of biogenic VOCs in smog chamber experiments conducted under high nitrogen oxide (NO_x) concentrations (Lin et al., 2012). These results indicate that coal combustion is an important source of nitrooxy-OS, and this conclusion was consistent with the results of previous studies (Song et al., 2018). As shown in Figure 4, a wide range of C number (6–32) and DBE values (3–23) were observed in this group, and the DBE value increased with the C number. The main compounds in this group were $O_7N_1S_1$, $O_{13}N_1S_1$ class species, with $O_7N_1S_1$ class species being the most abundant. It is worth noting that most of the H-CHONS compounds had DBE values greater than or equal to 4, and the compounds with high intensities in the H-CHONS groups detected from coal combustion were $C_6H_5O_7NS$ (5), $C_{10}H_7O_7NS$ (8), and $C_{10}H_6O_{11}N_2S$ (9). The most likely structure of these compounds is a benzene ring substituted with one sulfate and one or two nitrooxy groups (Song et al., 2018;Jiang et al., 2016). These were also detected in high concentrations in aerosols from Belgium and on a heavy $PM_{2.5}$ haze day in Beijing city (Jiang et al., 2016;Kahnt et al., 2013).

The presence of the P5 component was highly correlated with the L-CHOS group ($p < 0.05$). This group was mainly composed of O_3S and O_7S_2 class species from direct vehicle exhaust emissions. Generally, these compounds contained too little oxygen to form sulfate functional groups, containing reduced sulfur (S), such as

设置了格式 ...
设置了格式 ...
设置了格式: 检查拼写和语法
域代码已更改
设置了格式 ...
域代码已更改
设置了格式: 检查拼写和语法
带格式的: 首行缩进: 0 字符
域代码已更改
设置了格式 ...
域代码已更改
设置了格式 ...
域代码已更改
设置了格式 ...
设置了格式 ...
域代码已更改
域代码已更改
设置了格式 ...
设置了格式 ...

sulfonates, which was also detected in cloud water (Zhao et al., 2013). In these groups, the main compounds of $C_{26}H_{24}O_3S$ (15), $C_{27}H_{26}O_3S$ (15), and $C_{25}H_{22}O_3S$ (15) were homologues of $C_{24}H_{20}O_3S$ (15), with the same general formula, $C_nH_{2n-28}SO_3$, and DBE values, of 15, likely corresponding to sulfonates of substituted benzopyrene ($C_{20}H_{12}$, DBE=15) (Blair et al., 2017). However, the P2 and P3 components were not significantly correlated with these ion groups.

3.3.2 Composition of chromophores of MSOC

Figure 3b and Table S16 show the relationship between the relative intensity of the classified ions groups and the relative contents of the PARAFAC components of the MSOC fraction. Only the C1 and C3 components were associated with one ion group (H-CHOS and CHO_2>1, respectively). Considering that the C1 component was highly intense in the case of biomass burning, the H-CHOS groups observed in samples of biomass burning were O_5S_1, O_7S_1, $O_{10}S_2$, $O_{13}S_1$ class species, of which $O_{10}S_2$ was the most abundant family. The probable structure of these species is an organosulfate with other O-containing functional groups, such as hydroxyl or carboxyl groups. This groups had a narrow range of C numbers (12–16) and DBE values (8), such as $C_{14}H_{14}O_{10}S_2$ (8) and its homologues $C_{13}H_{12}O_{10}S_2$ (8), $C_{15}H_{16}O_{10}S_2$ (8), as well as $C_{15}H_{16}O_7S$ (8), $C_{16}H_{18}O_7S$ (8), $C_{12}H_{10}O_{13}S$ (8), and $C_{13}H_{12}O_{13}S$ (8).

C2 component was positively correlated with CHO_2>1, and negatively correlated with L-CHOS and L-CHONS groups. Figure 5 presented the DBE versus C number for the CHO_2>1 group from samples of biomass burning, with the main compounds had C numbers of 17–20, DBE (10–11), and O numbers of 4–5. The potential structures of $C_{18}H_{16}O_4$ (11) and $C_{17}H_{16}O_4$ (10) are indicated as a and b, respectively, in Figure 5 and are suspected to be cyclic esters. The L-CHOS group were mainly O4S2 class species, of which $C_{12}H_{10}O_4S_2$ (8) was the main formula. The possible chemical structure is of two S-heterocycles connected to two ester bonds. Thus, C2 components may relate to ester compounds.

Further, the C5 component was positively correlated with L-CHOS and L-CHONS groups ($p < 0.05$), and the C6 component was positively associated with

域代码已更改
设置了格式：检查拼写和语法
设置了格式 ...
设置了格式 ...
域代码已更改
设置了格式：检查拼写和语法
设置了格式：字体：非加粗
带格式的：段落间距段前：0 磅，段后：0 磅
设置了格式 ...
设置了格式 ...
设置了格式 ...
设置了格式 ...
设置了格式 ...
带格式的：首行缩进： 0 字符
设置了格式 ...
设置了格式 ...
设置了格式 ...

all S-containing groups ($p < 0.05$). We list some of the main formulas of these groups detected in direct vehicle exhaust (IDs: 59), such as $C_{12}H_{12}O_7S_2$ (7) and $C_{13}H_{14}O_7S_2$ (7) for L-CHOS groups; $C_{14}H_{14}O_{10}S_2$ (8) and $C_{15}H_{16}O_{10}S_2$ (8) for H-CHOS; $C_{36}H_{23}O_4NS$ (26) for L-CHONS; and $C_{10}H_6O_{11}N_2S$ (9), $C_{11}H_8O_{11}N_2S$ (9), $C_{10}H_7O_{13}NS$ (8), $C_{11}H_9O_{13}NS$ (8), $C_{12}H_{11}O_{13}NS$ (8) and $C_{12}H_8O_{14}N_2S$ (10) for H-CHONS. The L-CHOS groups containing two S atoms is potential to be formed by sulfonation reactions, and their possible structure is of a fused benzene ring substituted with two sulfonates (-SO_3H). $C_{36}H_{23}O_4NS$ may contain substantial quantities of S-containing compounds with reduced N (e.g., amide and nitrile, and heterocyclic aromatics) (Song et al., 2018). These results indicate that the C5 component is potentially related to sulfonates, but the structure of the C6 component is unclear. However, C4 components did not correlate with ion groups. Note that one class of compounds contributed to several fluorescent components, which indicated that numerous functional groups affect each component individually.

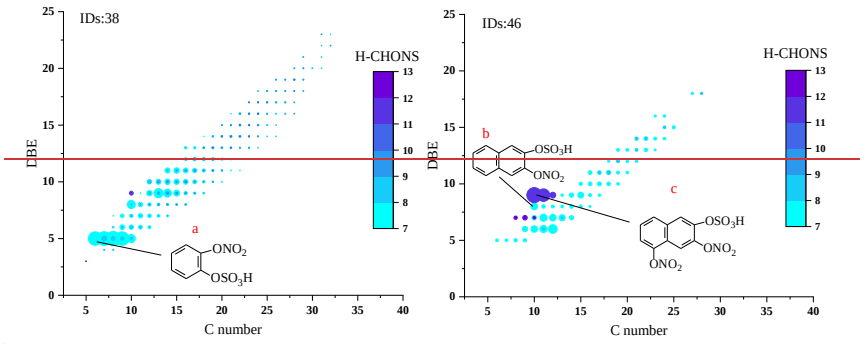

Figure 4. Double bond equivalent (DBE) versus C number for the H-CHONS group of WSOC of coal combustion samples. The color bar and marker size denote the number of O atoms and the relative intensities of the compounds; a: $C_6H_5O_7NS$ (DBE: 5); b: $C_{10}H_7O_7NS$ (8); and c: $C_{10}H_6O_{11}N_2S$ (9).

设置了格式
设置了格式
设置了格式
设置了格式
设置了格式
域代码已更改
设置了格式
设置了格式

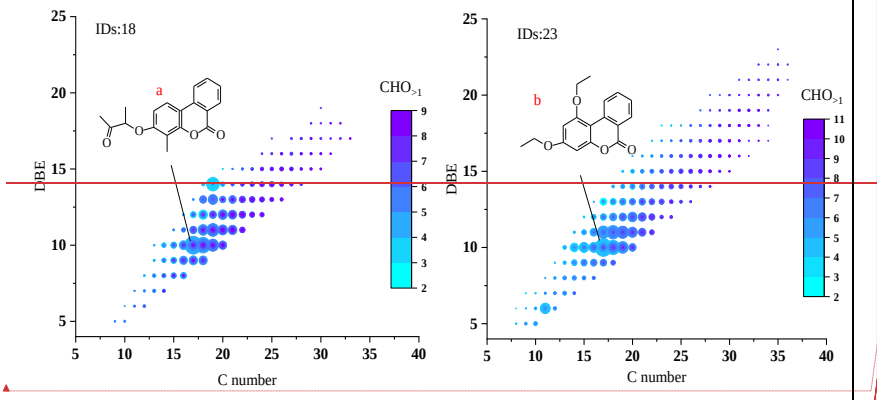

~~Figure 5. The DBE versus C number for the $CHO_{>1}$ group of MSOC of biomass burning samples. The color bar and marker size denote the number of O atoms and the relative intensities of the compounds, a: $C_{18}H_{16}O_4$ (11); b: $C_{17}H_{16}O_4$ (10).~~

The molecular composition of WSOC and MSOC extracted from BB and CC aerosols, and vehicle emissions were determined by negative ESI-FT-ICR MS. ESI is a soft ionization method, and it can only ionize polar organic compounds, hydrophilic molecules (Wozniak et al., 2008), but nonpolar or less polar compounds such as polycyclic aromatic hydrocarbons (PAHs) and saturated hydrocarbons are not easily ionized by ESI (Lin et al., 2018). In addition, ESI (-) cannot detect the N-heterocyclic alkaloid compounds (Laskin et al., 2009). Thus, this study mainly discussed these easily ionized polar organic compounds by ESI (-).

Figure 4 showed the reconstructed negative-ion ESI FT-ICR mass spectra of WSOC for the six selected samples. Lots of peaks with an intensive mass range between m/z 150 and 600 were shown in the spectra, with the most massive numbers of ions within the range of m/z 200-400. Additionally, more formulas were detected in BB aerosols (total 7708) than CC aerosols (5305) and vehicle emissions (4047) (Table 2), suggesting a higher observed chemical complexity (i.e., the observed peaks). According to the intensity of each ion, the average molecular formulas of WSOC in the six aerosol samples were calculated and listed as $C_{18.7}H_{23.5}O_{6.99}N_{0.73}S_{0.09}$, $C_{19.9}H_{21.5}O_{7.65}N_{0.34}S_{0.03}$, $C_{16.1}H_{13.3}O_{5.37}N_{0.68}S_{0.23}$, $C_{15.2}H_{13.7}O_{4.24}N_{0.45}S_{0.41}$, $C_{13.4}H_{18.0}O_{7.52}N_{0.45}S_{0.40}$, and $C_{17.3}H_{21.1}O_{5.65}N_{0.53}S_{0.08}$. The BB aerosols had higher

设置了格式 ...

带格式的：段落间距段前：0 磅，段后：0 磅，无孤行控制

带格式的：缩进：首行缩进： 2 字符，孤行控制

设置了格式 ...

contents of C and H, while the CC aerosols and tunnel aerosol had higher contents of S.

设置了格式：字体：小四，非加粗，英语(美国)

Table 2. Number of formulae in each compound category and the average values of elemental ratios, molecular weight (MW), double-bond equivalents (DBE), and aromaticity index (AI_{mod}) in the WSOC from the three origins.

带格式表格

Samples	Elemental composition	Number of formulae	MW_w	DBE_w	$AI_{mod,w}$	O/C_w	H/C_w	DBE/C
Musa	Total	4534	372.55	8.36	0.33	0.37	1.25	0.45
	CHO	1504	367.73	8.08	0.32	0.38	1.25	0.43
	CHON	2375	384.06	9.31	0.39	0.34	1.22	0.48
	CHOS	329	320.06	4.59	0.15	0.51	1.46	0.34
	CHONS	323	358.24	5.04	0.12	0.51	1.51	0.35
Hevea	Total	3174	387.05	10.32	0.42	0.38	1.08	0.52
	CHO	1610	377.86	10.06	0.42	0.38	1.08	0.51
	CHON	1408	409.40	11.29	0.46	0.39	1.05	0.55
	CHOS	108	376.68	7.00	0.23	0.38	1.32	0.39
	CHONS	48	410.33	5.08	0.09	0.47	1.60	0.30
Anthracite	Total	3930	308.65	10.82	0.65	0.33	0.83	0.67
	CHO	990	283.07	11.06	0.67	0.28	0.77	0.67
	CHON	1808	323.71	11.67	0.71	0.34	0.81	0.69
	CHOS	464	308.97	8.73	0.49	0.36	0.95	0.59
	CHONS	668	332.83	8.99	0.52	0.46	0.95	0.63
Bituminous coal	Total	1375	282.91	9.63	0.61	0.28	0.90	0.63
	CHO	399	259.21	10.40	0.66	0.22	0.82	0.65
	CHON	411	267.68	9.92	0.69	0.27	0.86	0.67
	CHOS	302	324.65	9.51	0.49	0.28	0.99	0.57
	CHONS	263	299.28	7.98	0.56	0.43	0.98	0.63
Tunnel	Total	2746	317.68	5.68	0.35	0.56	1.34	0.42
	CHO	803	298.29	7.69	0.49	0.50	1.06	0.54

	CHON	1049	340.18	7.50	0.38	0.51	1.22	0.49
	CHOS	508	310.74	2.73	0.03	0.59	1.71	0.23
	CHONS	386	337.90	2.78	0.46	0.81	1.77	0.25
Vehicle exhaust	Total	1301	327.71	7.96	0.41	0.33	1.22	0.46
	CHO	561	311.62	8.02	0.43	0.30	1.19	0.46
	CHON	673	320.62	7.28	0.41	0.40	1.27	0.47
	CHOS	63	467.88	11.88	0.36	0.19	1.19	0.44
	CHONS	4	438.78	2.21	0	0.46	1.97	0.12

In this study, these identified molecular formulas were classified into four main compound groups based on their compositions: CHO, CHON, CHOS, and CHONS. CHO compounds refer to the compounds that contained carbon, hydrogen, oxygen, and the other compound groups that were defined analogously. The relative abundances of the four compound groups were calculated by the magnitude of each peak divided by the sum of magnitudes of all identified peaks and showed in Figure 4. CHO was the most abundant component in the WSOC, accounting for 43% - 69% of total intensities of BB aerosols, 36% - 37% of CC aerosols, and 36% - 47% of vehicle emissions, respectively. CHO in the BB and CC aerosols were lower than those of mass spectra from simulated combustion experiments (BB (53%-72%) and CC (43%)) (Song et al., 2018). Generally, CHO formulas were consistent with species reported previously as lignin-pyrolysis products (Fleming et al., 2017), and they detected this fraction was 43.1% ± 14.6% in brushwood-chulha cook firers. CHON was abundant in the three sources. This result was different from the findings that CHON species had a higher percentage in BB smoke and were not abundant in CC smoke (Song et al., 2018). The high fraction of CHON in the CC aerosols could be due to that the N-containing compounds in the BB smoke $PM_{2.5}$ come from the nitrogen content in the fuels (Coggon et al., 2016), and the contents in coal fuels were comparable to biomass fuels (See Table S1 and S2). However, S-containing compounds were more abundant in the CC aerosols (9.0%-21% for CHOS and 13%-20% for CHONS, respectively) and tunnel aerosol (24% for CHOS and 16% for CHONS, respectively)

设置了格式：下标

than those in the BB aerosols (2.0%-5.6% for CHOS and 0.62%-3.7% for CHONS, respectively) and vehicle exhaust particle (7.5% for CHOS and 0.25% for CHONS, respectively), consistent with the previous studies (Song et al., 2018;Wang et al., 2017). ESI was more efficient in ionizing S-containing compounds and most of them were selectively ionized by ESI-, suggesting that they were polar species such as organosulfates (Lin et al., 2018). Our study reported that S-containing compounds in the WSOC were associated with CC emissions by combining with ^{14}C data (Mo et al., 2018). Furthermore, the relative abundances of group species in the CC aerosols and TA were similar to those of water extracts in the hazy day (Jiang et al., 2016), indicating both sources could be the important contributors of haze. However, differences between tunnel aerosol and vehicle exhaust particle were observed, indicating S-containing compounds in the tunnel aerosol were more secondary formation.

设置了格式：上标

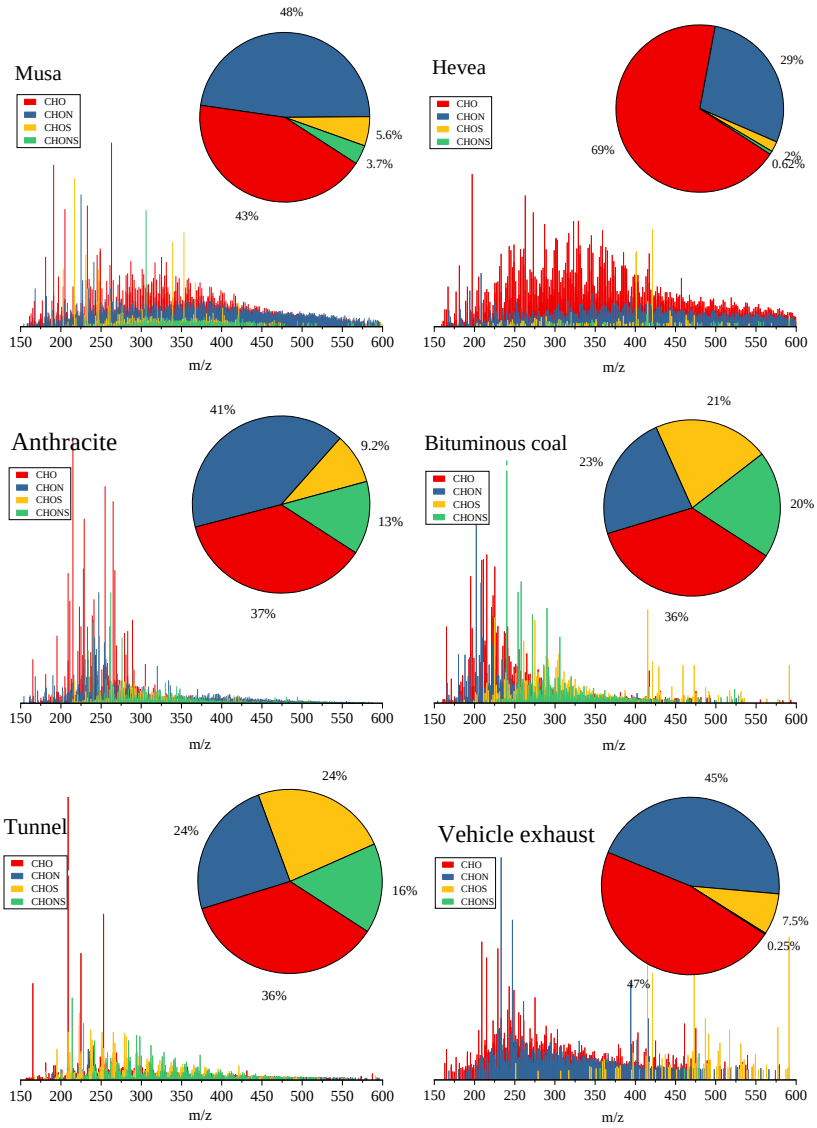

Figure 4. Negative ESI FT-ICR mass spectra of WSOC in the six aerosol samples. Different formula groups were color-coded. The six pie charts showed the relative intensities of different formula groups.

Van Krevelen (VK) diagram is a useful tool that provides a visual graphic display of compound distribution, and to some extent, use to qualitatively identify different composition domains in organic mixtures (Song et al., 2018;Lv et al., 2016;Smith et

带格式的：段落间距段后：0 磅

设置了格式：字体：五号，加粗

设置了格式：字体：五号

带格式的：缩进：首行缩进： 2 字符，段落间距段前：0 磅，段后：0 磅

al., 2009). In this study, each source showed similar VK patterns. Musa and Hevea burning had a resemble VK diagram to that of WSOC in straw burning and fog water (Schmitt-Kopplin et al., 2010;Mazzoleni et al., 2010). S-containing compounds in tunnel aerosol with high O/C and H/C ration were similar to the aerosol-derived WSOC in New York and Virginia (Wozniak et al., 2008). Six dominate domains were identified in the WSOC, including lignins, carbohydrates, tannins, proteins, condensed aromatic, and unsaturated hydrocarbons. As shown in Figure S9, results showed compounds observed in the CC aerosols had lower H/C and O/C ratios than those in the BB aerosols and vehicle emissions, indicating a higher unsaturated degree and lower oxidation level. There were compounds outside the specified regions, which had a high H/C ratio (≥2.2), and DBE = 0 correspond to saturated oxygenated species and could be some long-chain polyalcohols (Lin et al., 2012a).

The mass spectra of MSOC exhibited differences from WSOC (Figure S10), especially in the BB aerosols and vehicle emissions that exhibited larger m/z in the range of 350-600. The detected formulas in the MSOC were much lower than those in the WSOC, with the number of 4502, 3628, and 1069 for the BB, CC, and vehicle emission aerosols, respectively. The reason could be due to that ESI can efficiently ionize the polar compounds, and the methional extracts after water-extracted may contain more moderate- and low- polar compounds that were not easily ionized. The average molecular formulas were $C_{26.9}H_{46.2}O_{4.27}N_{0.24}S_{0.02}$, $C_{23.3}H_{34.9}O_{5.18}N_{0.20}S_{0.02}$, $C_{18.2}H_{19.2}O_{4.24}N_{0.92}S_{0.03}$, $C_{22.4}H_{20.7}O_{3.01}N_{0.38}S_{0.05}$, $C_{22.6}H_{44.1}O_{5.70}N_{0.74}S_{0.11}$, and $C_{25.2}H_{48.5}O_{4.86}N_{0.58}S_{0.08}$ of MSOC in the six aerosol samples, respectively, showing higher C and H contents than their corresponding formulas of WSOC but a decreasing trend in the O contents.

CHO and CHON were the main components in the MSOC, accounting for about 90% of the total intensities (CHO plus CHON). CHO was the most abundant category observed in the BB aerosols (78%-80%). The elemental compositions observed in CC aerosols were different between bituminous coal and anthracite combustion, where the latter had more abundance of CHON (73%), but the former with more CHO (60%), which was consistent with their corresponding WSOC and could be due to anthracite

设置了格式

设置了格式：下标

had higher N content but lower O content than bituminous coal (see Table S2). However, CHON in the BB aerosols (18%-20%) exhibited lower abundance than those in the CC aerosols and vehicle emissions. These results provided a new sight for those CHON compounds that contributed to a high abundance in fossil fuel combustion in the MSOC. Besides, S-containing compounds were not abundant in the MSOC. It is potential to due to that S element combined with O atom may exhibit higher polarity.

Figure S11 showed the VK diagram of MSOC in the six aerosol samples. More formulas in BB aerosols exhibited two distinct groups with H/C 1.4-2.2 and 0.6-1.4 vs. O/C 0.1-0.5, inside three domains (lignins, proteins, and lipids). Compounds in CC aerosols with lower H/C and O/C ratios were dominant in the domains of lignins and condensed aromatic, especially in the bituminous CC aerosol with more unsaturated hydrocarbon. Tunnel aerosol showed a wide range of O/C in S-containing compounds and a wide range of H/C in non-S-containing compounds. In contrast, compounds in vehicle exhaust particle had a wide range of H/C but a narrow O/C ratio. The VK diagram with fewer S-containing compounds in the vehicle exhaust particle showed a similar characteristic to the distribution of non-S-containing compounds in tunnel aerosol, indicating the difference was mainly due to the S-containing compounds.

Table 2 and S5 presented the relative abundance weighted molecular weight (MW_w), Double bonds equivalence (DBE_w), and modified aromaticity index ($AImod_w$) of WSOC and MSOC, respectively (see SI). DBE was used as a measure of unsaturated level in a moleculer, and AI_{mod} could be used to estimate the fraction of aromatic and condensed aromatic structures (Song et al., 2018;Lv et al., 2016;Koch and Dittmar, 2006). BB aerosols had higher MW_w values than CC and vehicle emissions in the WSOC. Besides, higher DBE_w and $AI_{mod,w}$ values were observed in the CC aerosols than the other two sources. MSOC had higher MW_w but lower AI_{mod} values (except for CC aerosols) than the corresponding WSOC. Furthermore, CHO and CHON compounds had higher DBE_w and $AI_{mod,w}$ values than S-containing substances, consistent with the earlier results (Lin et al., 2012b;Lin et al., 2012a).

设置了格式：下标
设置了格式：下标
设置了格式：下标
设置了格式：下标
设置了格式：下标
设置了格式：下标
设置了格式：下标
设置了格式：下标
设置了格式：下标
设置了格式：下标
设置了格式：下标

Figure S12 showed the fraction of AI_{mod} values of WSOC in the six aerosol samples, where the formulas were classified according to their AI_{mod} (aliphatic (AI = 0), olefinic (0 < AI ≤ 0.5) and aromatic (AI > 0.5)). The results illustrated that the fraction of aromatic structure in non-S-containing compounds was higher than those in S-containing compounds. CC aerosols had a higher aromatic fraction than BB aerosols and vehicle emissions, especially in CHO and CHON (up to 89% of total ion intensities). In the BB aerosols, the non-S-containing compounds had a high fraction of olefinic structure, following by aromatic structure, but the S-containing compounds had a higher aliphatic and olefinic structure than aromatic structure. Besides, a higher fraction of aliphatic in vehicle emissions was observed in S-containing compounds (especially in tunnel aerosol (exceed 81%)). These aliphatic S-containing compounds might form by the precursors (long-chain alkanes) from vehicle emissions (Tao et al., 2014), which had higher H/C and lower DBE values (see Table 2). However, the previous study showed that AI must be regarded as the most conservation approach and may result in an underestimate of the aromatic structures (Koch and Dittmar, 2006), which was observed in Beijing aerosols (Mo et al., 2018). Although AI_{mod} identified more compounds as aromatic and condensed aromatic components than AI, the AI_{mod} may introduce uncertainties for individual molecules, which was demonstrated by Koch and co-author.

Consistent with WSOC, high fractions of the aromatic structure were observed in non-S-containing compounds than S-containing compounds, and higher fractions of aromatic structure in the CC aerosols were observed than BB aerosols and vehicle emissions in the MSOC (Figure S13). Furthermore, we found that the fraction of aliphatic in MSOC was higher than that in WSOC, indicating more fat-like compounds.

Different chemical characteristic of BB, CC, and vehicle emissions

Figure S14 plotted the Venn diagram of formulas in the WSOC fraction in the six aerosol samples for determining the unique elementals in the mass spectra. The

设置了格式：下标
带格式的：缩进：首行缩进： 2 字符，段落间距段前：0 磅，段后：0 磅
设置了格式：下标
设置了格式
设置了格式：下标
设置了格式：下标
设置了格式：字体：倾斜

previous study identified the unique elementals of water-soluble HULIS in simulated BB and CC smokes, which presented different molecular characteristics between biomasses, as well as between biomass and coal (Song et al., 2018). In this study, we combined more formulas of different sources to determine the unique molecular and more limitation was set, which would provide more identified characteristics for each source. 212 molecular formulas were detected simultaneously in the six aerosol samples, suggesting the compounds could be more detected in the atmosphere. It is noting that without any further information, it is not possible to decide whether these common formulas represent the same compounds. There were 112 of CHO unique molecular in 212 and 98 of CHON but only 2 of CHOS molecular. CHO compounds were relatively small aromatic compounds with 8-10 C atoms and 3-8 O atoms and DBE 5-13 and multiple acidic polar functional groups (Figure S15). It is noting that lines in Figure S15 indicate DBE reference values of linear conjugated polyenes CxHx+2 with DBE=0.5×C, and fullerene-like hydrocarbons with DBE=0.9×C, where the data points inside this region are potential BrC chromophores (Lin et al., 2018). For example, organic acids ($C_8H_6O_5$ (DBE=6) was detected in Urban $PM_{2.5}$ (Yassine et al., 2012), as well as $C_9H_8O_5$ (6), $C_{14}H_{14}O_4$ (8), $C_{13}H_{14}O_5$ (7), which allowed them to ionization in the ESI- mode and were identified as potential BrC chromophores. In total, all of CHON compounds had O/N≥2 (5.3±1.28, 2.5-7) (Figure S15), allowing for the assignment of at least one nitro ($-NO_2$) or nitrooxy ($-ONO_2$) group and other oxygen-containing groups (i.e., -OH and -COOH). Except for $C_{19}H_{41}O_7N$ (DBE=0), the remaining compounds with DBE≥5 were suggested as nitro-aromatic and nitrophenol derivatives (Mo et al., 2018;Lin et al., 2018). CHOS species only had two formulae including $C_{18}H_{38}O_7S$ (0) and $C_{20}H_{38}O_7S$ (2). It was reported that O_7S groups were the most abundant species class in CHOS identified in water extracts of $PM_{2.5}$ (Jiang et al., 2016).

There were more observed unique peaks of WSOC in the BB aerosols (total 1947) compared to CC aerosols (1583) and vehicle emissions (813). However, only 143 and 83 molecular were identified in bituminous CC and vehicle exhaust particle,

设置了格式：下标
设置了格式：下标
设置了格式：下标
设置了格式：下标
设置了格式：下标
设置了格式：下标
设置了格式：下标
设置了格式：下标
设置了格式：下标
设置了格式：下标
设置了格式：下标
设置了格式：下标
设置了格式
设置了格式：下标
设置了格式：下标
设置了格式：下标
设置了格式：下标
设置了格式：下标
设置了格式
设置了格式：下标
设置了格式：下标
设置了格式：下标
设置了格式：下标
设置了格式：下标
设置了格式：下标
设置了格式：下标
带格式的：段落间距段前：0.5 行，段后：0 磅

831 respectively. Among the observed compounds, 1353 and 1440 unique molecular
832 formulas were detected in in combustion of Musa and anthracite, respectively,
833 showing a significant difference from the others. Figure 5 (a) showed the VK diagram
834 of these unique formulas of WSOC for each sample, where four regions were circled
835 for representing different sources. The results indicated that these unique compounds
836 in different sources had a distinctive chemical characteristic. That may be the reason
837 that resulted in variable fluorescent spectra in different sources (discussed above).
838 Additionally, the diagram showed that the unique molecular in CC aerosols located in
839 the region with lower H/C and O/C, and vehicle emissions between tunnel aerosol and
840 vehicle exhaust particle located in two distinct regions.
841 Figure 6 showed plots of the DBE vs. the number of carbon atoms in the unique
842 molecular formulas of all aerosol samples. These compounds observed in the BB
843 aerosols were largely CHO and CHON (CHO and CHON, 88% - 93%) with C
844 numbers ranging from 6 to 40 and DBE ranging from 0 to 31, with no regular
845 distribution. S-containing compounds were the important components in the unique
846 molecular formulas of CC aerosols (CHOS and CHONS, 38%-75%) and vehicle
847 emissions (CHOS and CHONS, 41%-66%). However, only 7%-12% of the total
848 unique molecular formulas were observed in BB aerosols. As shown in Figure 6, the
849 region marked by blue box denoted the high intensities of compounds in unique
850 formulas of each sample. The high-intensity compounds detected in the Musa burning
851 aerosol were mainly C number from 14 to 24, DBE from 7 to 13, and two N atoms,
852 such as $C_{20}H_{26}O_7N_2$ (9), $C_{18}H_{24}O_2N_2$ (8), $C_{22}H_{28}O_6N_2$ (10), $C_{19}H_{26}O_7N_2$ (8),
853 $C_{21}H_{28}O_6N_2$ (7), $C_{14}H_{18}O_7N_2$ (7), $C_{24}H_{30}O_8N_2$ (11), and $C_{21}H_{24}O_5N_2$ (11) and so on.
854 Instead of Musa, the abundant compounds in the Hevea were mainly $C_{24}H_{22}O_9$ (14),
855 $C_{28}H_{28}O_{11}$ (15), and $C_{28}H_{26}O_{11}$ (16), and so on. Although the difference between
856 burning of Musa and Hevea appeared, the VK diagram (Figure 5) did not show
857 distinct changes. The high-intensity compounds in the anthracite combustion with
858 lower C atoms than in the bituminous CC, which were main $C_{14}H_8O_5N_2$ (12),
859 $C_{12}H_{11}O_4NS$ (8), $C_{12}H_{10}O_8N_2$ (9), while in bituminous CC were main $C_{28}H_{28}O_4S$ (15)
860 and its homolog of $C_{27}H_{26}O_4S$ (15), and $C_{19}H_{16}O_3S$ (12). The abundant compounds in

带格式的: 缩进：首行缩进： 2 字符，段落间距段前：0 磅，段后：0 磅

设置了格式 ...

设置了格式 ...

tunnel aerosol had a lower unsaturation degree, such as $C_4H_9O_7NS$ (1), $C_5H_{11}O_7NS$ (1), $C_7H_{13}O_5S$ (1). In the vehicle exhaust particle, the high intensity of compounds was one fraction with low C atoms and DBE ($C_{21}H_{40}O_8N_2S$ (3), $C_{26}H_{46}O_3S$ (4)), and the other fraction with high C atoms and DBE ($C_{32}H_{34}O_8S$ (16), $C_{30}H_{34}O_5S$ (14)). These findings are essential because these unique molecular formulas in different sources may have specific chemical composition, which would help the source apportionment of aerosols.

设置了格式：下标

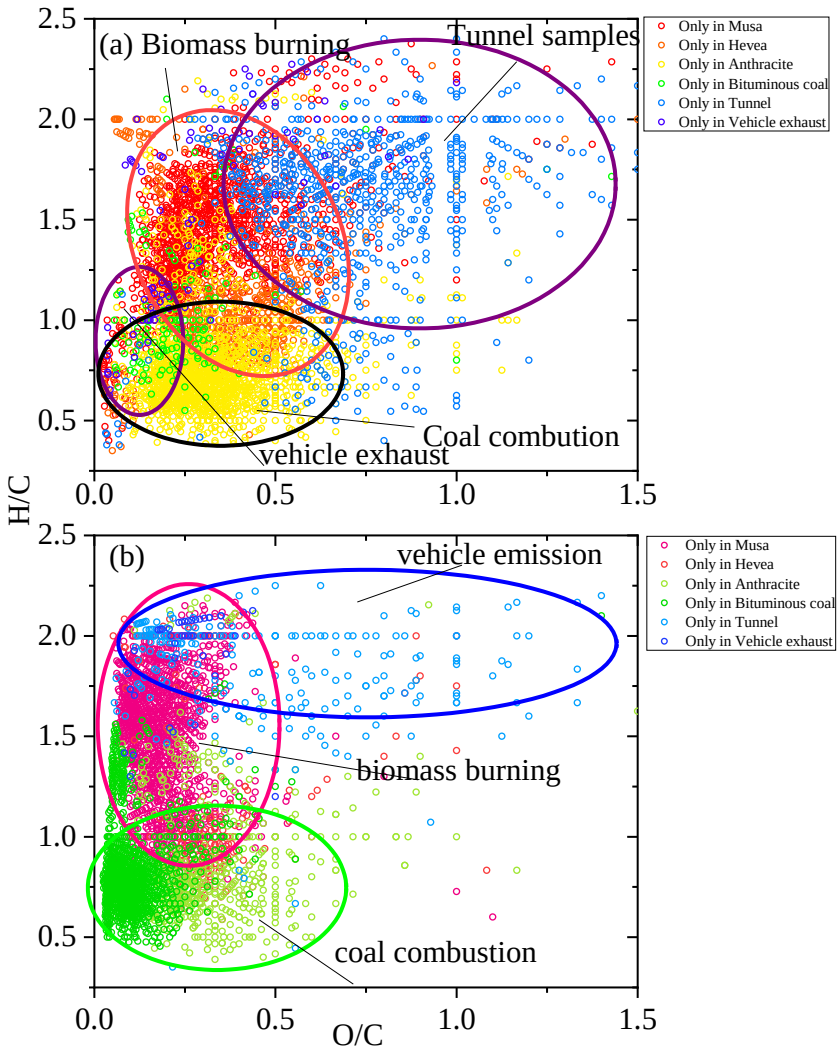

868

869 Figure 5. A Van Krevelen diagram of WSOC (a) and MSOC (b) in the six samples.

870 Different color indicates unique formulas detected in each sample.

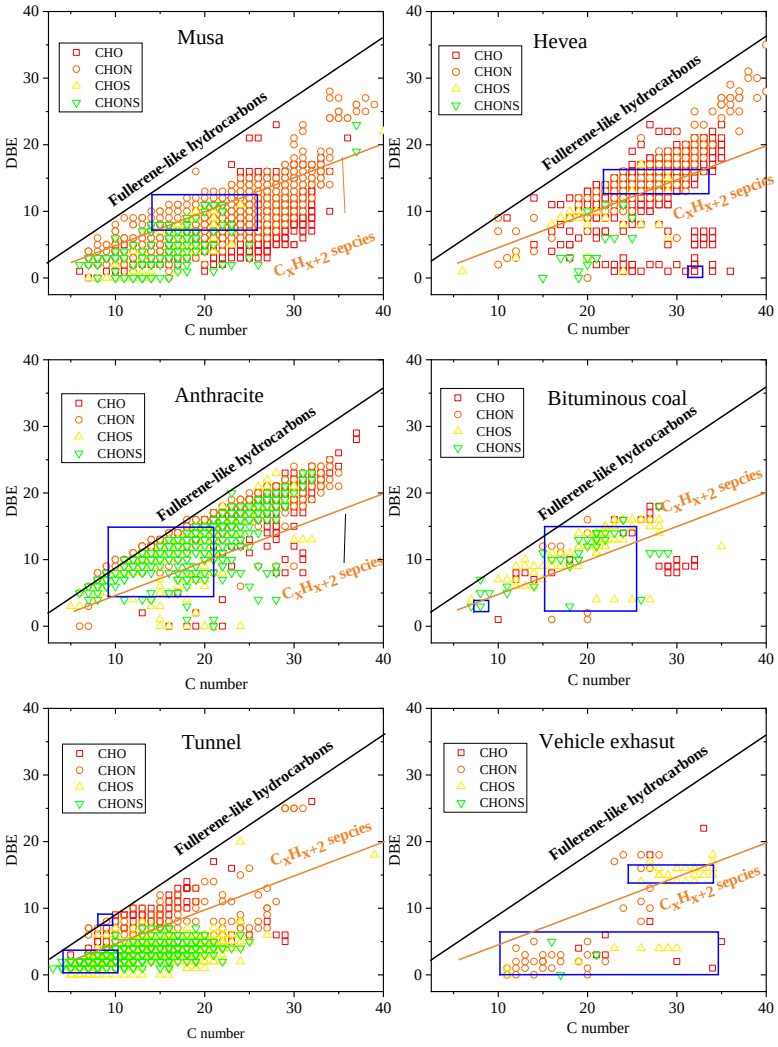

871

872 Figure 6. DBE vs. C number for unique molecular compounds of WSOC for the six aerosol

873 samples. Lines indicate DBE reference values of linear conjugated polyenes C_xH_{x+2} with

874 DBE=0.5×C, and fullerene-like hydrocarbons with DBE=0.9×C. The regions marked by blue box

875 denoted the high intensities of compounds.

876 Comparison with WSOC, Figure S16 showed fewer compounds in common in

877 the MSOC for the six aerosol samples. There were only 44 compounds common in the

设置了格式：字体：五号

带格式的：段落间距段前：0 磅，段后：0 磅

设置了格式：字体：五号，下标

设置了格式：字体：五号

设置了格式：字体：五号，下标

设置了格式：字体：五号

带格式的：缩进：首行缩进： 2 字符，段落间距段前：0 磅，段后：0 磅

six aerosol samples. A total of 26 and 14 of the 44 formulas were CHO and CHON, respectively, but only 4 of the 44 formulas were S-containing compounds. As shown in Figure S17, there were only three compounds ($C_{17}H_8O_2$ (13), $C_{18}H_{14}O$ (12), $C_{18}H_{12}O_2$ (13)) in CHO group, and one compound ($C_{14}H_{11}O_4N$ (10)) in CHON group inside the potential BrC region. The remaining compounds had a high C number (18-35), low O atoms (1-7), and low DBE (0-2), suggesting that they mostly had fatty acid structures.

These unique molecular in VK also showed similar results comparing to WSOC (Figure 5 (b)), further confirming the special characters in different sources. Expect for tunnel aerosol (about 50%), these unique formulas in the BB aerosols, CC aerosols, and vehicle exhaust particle was dominant by CHO- and CHON-groups (Figure S18), indicating S-containing compounds with lower polarity could be originated from the secondary formation of vehicle exhaust. The high-intensity compounds were $C_{35}H_{69}O_5N$ (2), $C_{38}H_{76}O_4$ (1) for Musa burning; $C_{26}H_{22}O_7$ (16), $C_{28}H_{26}O_7$ (16) for Hevea burning; $C_{14}H_{12}O_6N_2$ (10), $C_{17}H_{14}O_5N_2$ (12) for anthracite combustion; $C_{23}H_{16}O$ (16), $C_{24}H_{18}O$ (16), $C_{24}H_{14}O$ (18) for bituminous CC; $C_4H_9O_7NS$(1),$C_{24}H_{42}O_3S$ (4), $C_8H_{16}O_5S$ (1) for tunnel aerosol, and $C_{26}H_{37}O_5NS$(7), $C_{22}H_{46}O_7$(0) for vehicle exhaust particle, respectively.

3.4 Link of molecular composition and optical properties

In the above statements, we discussed the light absorption and fluorescence properties from aerosols in the three different sources. The light absorption capacity of WSOC and MSOC was essential to assess the evolution of BrC, and fluorescence spectra were sensitive to different sources and could help for the source apportionment of BrC. Besides, we evaluated the molecular composition of the three sources. Therefore, understanding the factors affecting the optical properties of BrC is important. It was reported that the MAE in the BB experiments depended largely on burning conditions (Chen and Bond, 2010) and in the CC experiments depended on coal maturity (Li et al., 2018). Chen et al., (2017b) illustrated that higher light absorption capacity were

设置了格式：字体：（默认）Times New Roman，英语(美国)，下标

设置了格式：字体：（默认）Times New Roman，英语(美国)，下标

设置了格式：字体：（默认）Times New Roman，英语(美国)，下标

设置了格式：字体：加粗

associated with low- and medium-polar fractions that contained aromatic and polar functional groups (O or both O and N atoms). Sources play an important role in light absorption capacity, consistent with our current study. The MAE_{365} values of WSOC in highly BB-impacted areas were two times higher than in low BB-impacted areas in the Southeastern United States (Hecobian et al., 2010). Atmospheric aging has a significant effect on the light absorption capacity of BrC (Li et al., 2019), but the mechanism involved is very complex. The response of the light absorption capacity of different types of BrC to aging is highly variable, and enhancement or reduction in the light absorption capacity of BrC is possible (Li et al., 2019). These results indicated that light absorption capacity might be affected by various factors. In this study, higher MAE_{365} values were observed in the BB and CC aerosols than vehicle emissions, and the chemical structures and unsaturation degree of different sources were discussed. Next, we further discussed the relationships between optical properties and chemical structures.

In order to reduce the influence of non-absorbing substances, we firstly determined these compounds, which were potential to absorb light radiation based on the above statement. Mo et al., (2018) reported that MAE_{365} of HULIS in aerosols was affected by oxidation level and unsaturation degree. In this study, the MAE_{365} had no significant correlation with O/C, indicating that light absorption capacity does not appear to be affected by their oxidized properties in the source aerosols. Instead of O/C, the MAE_{365} had a well positive correlation with the average DBE and MW, respectively (Figure 7), suggesting the unsaturation level and MW played a vital role in the light absorption capacity of source samples. Field experiments indicated that the majority of absorption was the larger molecules (>500 Da) (Di Lorenzo et al., 2017). It is crucial to knowledge the relationship between light absorption of source samples and their chemical structures due to the compounds in fresh emissions that may undergo a secondary process and introduce more uncertainty for their optical properties.

设置了格式：下标

设置了格式：下标

设置了格式：下标

设置了格式：下标

设置了格式：下标

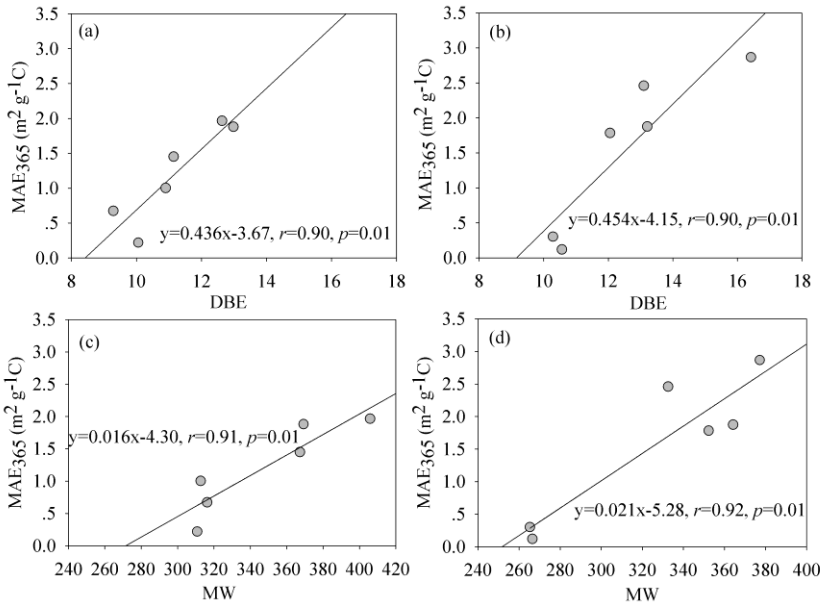

Figure 7. Relationship between DBE and MW of the potential BrC molecules and the MAE365 of WSOC (a, c) and MSOC (b, d) in the six samples, respectively.

Fluorescence spectra could provide more information than UV-vis spectra. A red shift in the excitation/emission maximum could indicate increased aromaticity and higher molecular weight (Ghidotti et al., 2017). Field observation had demonstrated that chromophore components were associated with chemical structures (Chen et al., 2016b;Chen et al., 2016a;Stubbins et al., 2014). Chen et al., (2016b) illustrated that the fluorescent components of HULIS-1 and HULIS-2 were correlated positively with CO_x^+ and CO_{2x}^+, and $C_xH_y^+$ and $C_xH_yO_1^+$ groups ions, respectively, using the correlation analysis of the relative intensities of ion groups in the high-resolution aerosol mass spectrometers (HR-AMSs) and relative contents of fluorescence components. In another study, Chen et al., (2016a) demonstrated that fluorescent components had strong links with chemical groups in the Fourier transform infrared (FT-IR) spectra, including the oxygenated functional groups (nonacidic carbonyl C=O and carboxylic COOH groups), aliphatic C-H group, amine C-NH2, and alcohol

带格式的：缩进：首行缩进： 2 字符

设置了格式：上标
设置了格式：下标
设置了格式：上标
设置了格式：下标
设置了格式：下标
设置了格式：上标
设置了格式：下标
设置了格式：下标
设置了格式：下标
设置了格式：上标

C-OH groups. The chromophores are sensitive to sources, and it is very important to understand the molecular composition of chromophores for classification and source apportionment of atmospheric BrC. However, the ESI- cannot ionize the most typical BrC chromophores such as O-heterocyclic PAHs (O-PAHs), N-heterocyclic PAHs (O-PAHs) (Lin et al., 2018), which was not enough to discuss the relationship between the fluorescence spectra and molecular composition. The combination of atmospheric pressure photoionization (APPI+ and APPI -) and ESI (+ and -) may provide more ionized compounds, but these techniques were not with the scope of our study.

4 Conclusions

We conducted comprehensive measurements on light absorption, fluorescence, and molecular compositions of dissolved BrC derived from smoke particles during the simulated combustion of biomass and coal, as well as vehicle emissions. We observed ~~the~~ BB and CC aerosols had high MAE_{365} values than vehicle emissions, on average, 1.6 ± 0.55, 1.3 ± 0.34, 2.0 ± 0.75, and 0.71 ± 0.30 m2 g-1 C for BB, anthracite combustion, bituminous CC and vehicle emission aerosols, respectively. In addition, BrC emitted from BB (2.3 ± 1.1 m^2 g^{-1} C) and bituminous CC (3.2 ± 1.1 m^2 g^{-1} C) in the MSOC exhibited stronger light absorption capacity than those in the WSOC, but opposite results were found in anthracite combustion aerosols (0.88 ± 0.74 m^2 g^{-1} C) and vehicle emissions (0.26 ± 0.09 m^2 g^{-1} C). ~~optical properties of the WSOC and MSOC fractions and observed that the light absorption of methanol-soluble BrC was stronger.~~ EEM combining with PARAFAC analysis determined ~~Six~~ six types of fluorescent components that were assigned as two HULIS-1 (P1, and P6), three PLOM (P2, P3, P5), and one undefinition (P4) in the WSOC in the source samples.~~were resolved in the WSOC and MSOC fractions by PARAFAC analysis, respectively.~~ The relative intensities of the fluorescent components ~~of the WSOC and MSOC fractions~~ mainly depended on the different types of ~~smoke particles~~sources, For example, HULIS-1 was abundant in tunnel aerosols, P2 was more intense in BB aerosols but not observed in vehicle emissions, P4 was intense in CC aerosols and vehicle emissions, P5 was more abundant in the fresh vehicle exhaust particles;

设置了格式：字体：非加粗

设置了格式：下标

设置了格式：上标

设置了格式：上标

设置了格式：上标

设置了格式：上标

设置了格式：上标

设置了格式：上标

设置了格式：上标

设置了格式：上标

although P3 was not abundant it was ubiquitous in all tested aerosols. Similar to WSOC, six fluorescent components were identified in MSOC. Although the methanol-soluble chromophores were poorly understood, different characteristics were observed in different sources.~~which were derived from several origins, suggesting that the fluorescent components varied from source to source. This result may be useful for fluorescence based methods, which play an important role in the classification and source identification of BrC dissolved in the atmosphere.~~

~~We also discussed the possible structures of these chromophores. Our results indicate that these fluorescent components were mainly affected by functional groups, especially functional groups containing N and S. In the case of the WSOC fraction, P1 and P6 components were mainly associated with aromatic organosulfate compounds; the P4 and P5 components were mainly associated with nitrooxy-OS compounds and sulfonates, respectively. However, we did not elucidate the structures of the P2 and P3 components. In the case of the MSOC fraction, the C1 component was mainly related to organsulfate compounds; the C3 component was related to $CHO_{>1}$ groups; the C2 component was mainly correlated with esters; and the C5 component was related to sulfonates. The C6 component was correlated well with S-containing compounds. As with the P2 and P3 components, we know little about the structure of the C4 component. Our findings provide insights into the chemical structures of water- and methanol-soluble chromophores, and these results may be useful for further aerosol studies, for source apportionment of dissolved BrC based on EEM fluorescence.~~

FT-ICR mass spectra showed that the m/z of the mainly compounds with m/z 200-400 in the WSOC and MSOC were m/z 350-600 (except for CC aerosols), respectively. CHO and CHON were the main components in the three origins, but S-containing compounds were more abundant in CC and tunnel aerosols than BB aerosol and vehicle exhaust particles in the WSOC. Similarily, MSOC mainly also contained CHO and CHON species but fewer S-containing compounds. BB aerosols had higher CHO species in MSOC but showed lower CHON than CC aerosols and vehicle emissions. Ven diagram showed that CC aerosols had more unsaturation

带格式的：段落间距段前：1 行

degree and low oxidation level than the other two sources. This finding was further confirmed by a higher fraction of aromatic in CC aerosols. Unique formulas determined by Venn diagram showed certain specific chemical characteristics in VK diagram. BB aerosols emitted unique formulas with more CHO and CHON (88%-93%), while CC aerosols and vehicle emissions contained more S-containing compounds (38%-75% and 41%-46%, respectively). The relationship between optical properties and chemical structures showed the light absorption capacity was positively associated with an unsaturation degree and MW in the source emissions. Our study illustrated the important roles of sources in light-absorbing BrC and molecular compositions and the EEM-based method is handy for classification and source apportionment of chromophores in atmospheric aerosols.

Data availability. The data used in this study are available upon request; please contact Gan Zhang (Zhanggan@gig.ac.cn) and Jun Li (junli@gig.ac.cn)

Supplement. The supplement related to this article is available.

Author contributions. JT, GZ, JL, and YC designed the experiment. JT and MC carried out the measurements and analyzed the data. JT, TS, YH, and HJ organized and performed the samplings. JT (Jianhui Tang) and BJ supported the fluorescence and FT-ICR MS instrument. JT wrote the paper. JL, YM, JS, PP, and GZ reviewed and commented on the paper.

Competing interests. The authors declare that they have no conflict of interest.

Acknowledgements. This study was supported by the Natural Science Foundation of China (NSFC; Nos. 41430645 and 41773120), the National Key R&D Program of China (2017YFC0212000), and the International Partnership Program of Chinese Academy of Sciences (Grant No.132744KYSB20170002).

Reference:

Alexander, L., Smith, J. S., and Julia, L.: Molecular characterization of nitrogen-containing organic compounds in biomass burning aerosols using high resolution mass spectrometry, Environ. Sci. Technol., 43, 3764-3771, https://doi.org/10.1021/es803456n, 2009.

Andersson, C. A., and Bro, R.: The N-way Toolbox for MATLAB, Chemom. Intell. Lab. Syst., 52, 1-4, https://doi.org/10.1016/s0169-7439(00)00071-x, 2000.

Andrade-Eiroa, Á., Canle, M., and Cerdá, V.: Environmental Applications of Excitation-Emission Spectrofluorimetry: An In-Depth Review I, Appl. Spectrosc. Rev., 48, 1-49, https://doi.org/10.1080/05704928.2012.692104, 2013.

Bahram, M., Bro, R., Stedmon, C., and Afkhami, A.: Handling of Rayleigh and Raman scatter for PARAFAC modeling of fluorescence data using interpolation, J. Chemom., 20, 99-105, https://doi.org/10.1002/cem.978, 2006.

Bhattacharya, R., and Osburn, C. L.: Multivariate Analyses of Phytoplankton Pigment Fluorescence from a Freshwater River Network, Environ. Sci. Technol., 51, 6683-6690, https://doi.org/10.1021/acs.est.6b05880, 2017.

Budisulistiorini, S. H., Riva, M., Williams, M., Chen, J., Itoh, M., Surratt, J. D., and Kuwata, M.: Light-Absorbing Brown Carbon Aerosol Constituents from Combustion of Indonesian Peat and Biomass, Environ. Sci. Technol., 51, 4415-4423, https://doi.org/10.1021/acs.est.7b00397, 2017.

Blair, S. L., MacMillan, A. C., Drozd, G. T., Goldstein, A. H., Chu, R. K., Pasa-Tolic, L., Shaw, J. B., Tolic, N., Lin, P., Laskin, J., Laskin, A., and Nizkorodov, S. A.: Molecular Characterization of Organosulfur Compounds in Biodiesel and Diesel Fuel Secondary Organic Aerosol, Environ. Sci. Technol., 51, 119-127, https://doi.org/10.1021/acs.est.6b03304, 2017.

Chen, H., Liao, Z. L., Gu, X. Y., Xie, J. Q., Li, H. Z., and Zhang, J.: Anthropogenic Influences of Paved Runoff and Sanitary Sewage on the Dissolved Organic Matter Quality of Wet Weather Overflows: An Excitation-Emission Matrix Parallel Factor Analysis Assessment, Environ. Sci. Technol., 51, 1157-1167, https://doi.org/10.1021/acs.est.6b03727, 2017a.

Chen, Q., Ikemori, F., and Mochida, M.: Light Absorption and Excitation-Emission Fluorescence of Urban Organic Aerosol Components and Their Relationship to Chemical Structure, Environ. Sci. Technol., 50, 10859-10868, https://doi.org/10.1021/acs.est.6b02541, 2016a.

Chen, Q., Miyazaki, Y., Kawamura, K., Matsumoto, K., Coburn, S., Volkamer, R., Iwamoto, Y., Kagami, S., Deng, Y., Ogawa, S., Ramasamy, S., Kato, S., Ida, A., Kajii, Y., and Mochida, M.: Characterization of Chromophoric Water-Soluble Organic Matter in Urban, Forest, and Marine Aerosols by HR-ToF-AMS Analysis and Excitation-Emission Matrix Spectroscopy, Environ. Sci. Technol., 50, 10351-10360, https://doi.org/10.1021/acs.est.6b01643, 2016b.

Chen, Q., Ikemori, F., Nakamura, Y., Vodicka, P., Kawamura, K., and Mochida, M.: Structural and Light-Absorption Characteristics of Complex Water-Insoluble Organic Mixtures in Urban Submicrometer Aerosols, Environ. Sci. Technol., 51, 8293-8303, https://doi.org/10.1021/acs.est.7b01630., 2017b.

Chen, Q., Mu, Z., Song, W., Wang, Y., Yang, Z., Zhang, L., and Zhang, Y. L.: Size - Resolved Characterization of the Chromophores in Atmospheric Particulate Matter From a Typical Coal - Burning City in China, Journal of Geophysical Research: Atmospheres, 124, 10546-10563, https://doi.org/10.1029/2019jd031149, 2019.

Chen, Y., Sheng, G., Bi, X., Feng, Y., Bixian Mai, A., and Fu, J.: Emission Factors for Carbonaceous Particles and Polycyclic Aromatic Hydrocarbons from Residential Coal Combustion in China, Environ. Sci. Technol., 39, 1861-1867, https://doi.org/10.1021/es0493650, 2005.

Chen, Y., and Bond, T. C.: Light absorption by organic carbon from wood combustion, Atmos. Chem. Phys., 10, 1773-1787, 10.5194/acp-10-1773-2010, 2010.

~~Chen, Y., and Bond, T. C.: Light absorption by organic carbon from wood combustion, Atmos. Chem. Phys., 10, 1773-1787, https://doi.org/10.5194/acp-10-1773-2010, 2009.~~

Chen, Y., Tian, C., Feng, Y., Zhi, G., Li, J., and Zhang, G.: Measurements of emission factors of PM2.5, OC, EC, and BC for household stoves of coal combustion in China, Atmos. Environ., 109, 190-196, https://doi.org/10.1016/j.atmosenv.2015.03.023, 2015.

Chen, Y., Ge, X., Chen, H., Xie, X., Chen, Y., Wang, J., Ye, Z., Bao, M., Zhang, Y., and Chen, M.: Seasonal light absorption properties of water-soluble brown carbon in atmospheric fine particles in Nanjing, China, Atmos. Environ., 230-240, https://doi.org/10.1016/j.atmosenv.2018.06.002, 2018.

Cheng, Y., He, K. B., Zheng, M., Duan, F. K., Du, Z. Y., Ma, Y. L., Tan, J. H., Yang, F. M., Liu, J. M., Zhang, X. L., Weber, R. J., Bergin, M. H., and Russell, A. G.: Mass absorption efficiency

of elemental carbon and water-soluble organic carbon in Beijing, China, Atmos. Chem. Phys., https://doi.org/11, 11497-11510, 10.5194/acp-11-11497-2011, 2011.

Cheng, Y., He, K.-b., Du, Z.-y., Engling, G., Liu, J.-m., Ma, Y.-l., Zheng, M., and Weber, R. J.: The characteristics of brown carbon aerosol during winter in Beijing, Atmos. Environ., 127, 355-364, https://doi.org/10.1016/j.atmosenv.2015.12.035, 2016.

Coble, P. G.: Characterization of marine and terrestrial DOM in seawater using excitation-emission matrix spectroscopy, Mar. Chem., 51, 325-346, https://doi.org/10.1016/0304-4203(95)00062-3, 1996.

Coggon, M. M., Veres, P. R., Yuan, B., Koss, A., Warneke, C., Gilman, J. B., Lerner, B. M., Peischl, J., Aikin, K. C., Stockwell, C. E., Hatch, L. E., Ryerson, T. B., Roberts, J. M., Yokelson, R. J., and de Gouw, J. A.: Emissions of nitrogen-containing organic compounds from the burning of herbaceous and arboraceous biomass: Fuel composition dependence and the variability of commonly used nitrile tracers, Geophys. Res. Lett., 43, 9903-9912, 10.1002/2016gl070562, 2016.

Cory, R. M., and Mcknight, D. M.: Fluorescence Spectroscopy Reveals Ubiquitous Presence of Oxidized and Reduced Quinones in Dissolved Organic Matter, Environ. Sci Technol., 39, 8142-8149, https://doi.org/10.1021/es0506962, 2005.

Cui, M., Chen, Y., Zheng, M., Li, J., Tang, J., Han, Y., Song, D., Yan, C., Zhang, F., Tian, C., and Zhang, G.: Emissions and characteristics of particulate matter from rainforest burning in the Southeast Asia, Atmos. Environ., 191, 194-204, https://doi.org/10.1016/j.atmosenv.2018.07.062, 2018.

Dasari, S., Andersson, A., Bikkina, S., Holmstrand, H., Budhavant, K., Satheesh, S. K., Asmi, E., Kesti, J., Backman, J., and Salam, A.: Photochemical degradation affects the light absorption of water-soluble brown carbon in the South Asian outflow, Science Advances, 5, https://doi.org/10.1126/sciadv.aau8066, 2019.

~~Dai, S., Bi, X., Chan, L. Y., He, J., Wang, B., Wang, X., Peng, P., Sheng, G., and Fu, J.: Chemical and stable carbon isotopic composition of PM2.5 from on-road vehicle emissions in the PRD region and implications for vehicle emission control policy, Atmos. Chem. Phys., 15, 3097-3108, https://doi.org/10.5194/acp-15-3097-2015, 2015.~~

Di Lorenzo, R. A., Washenfelder, R. A., Attwood, A. R., Guo, H., Xu, L., Ng, N. L., Weber, R. J.,

Baumann, K., Edgerton, E., and Young, C. J.: Molecular-Size-Separated Brown Carbon Absorption for Biomass-Burning Aerosol at Multiple Field Sites, Environ. Sci. Technol., https://doi.org/10.1021/acs.est.6b06160, 2017.

Fan, X., Song, J., and Peng, P. a.: Comparison of isolation and quantification methods to measure humic-like substances (HULIS) in atmospheric particles, Atmos. Environ., 60, 366-374, https://doi.org/10.1016/j.atmosenv.2012.06.063, 2012.

Fan, X., Wei, S., Zhu, M., Song, J., Peng, P: Comprehensive characterization of humic-like substances in smoke PM2.5 emitted from the combustion of biomass materials and fossil fuels, Atmos. Chem. Phys., 16, 13321-13340, https://doi.org/ 10.5194/acp-16-13321-2016, 2016.

Feng, S., Zhang, L., Wang, S., Nadykto, A. B., Xu, Y., Shi, Q., Jiang, B., and Qian, W.: Characterization of dissolved organic nitrogen in wet deposition from Lake Erhai basin by using ultrahigh resolution FT-ICR mass spectrometry, Chemosphere, 156, 438-445, https://doi.org/10.1016/j.chemosphere.2016.04.039, 2016.

Feng, Y., Ramanathan, V., and Kotamarthi, V. R.: Brown carbon: a significant atmospheric absorber of solar radiation?, Atmos. Chem. Phys., 13, 8607-8621, https://doi.org/10.5194/acp-13-8607-2013, 2013.

Fleming, L. T., Lin, P., Laskin, A., Laskin, J., Weltman, R., Edwards, R., Arora, N. K., Yadav, A., Meinardi, S., and Blake, D. R.: Molecular Composition of Particulate Matter Emissions from Dung and Brushwood Burning Household Cookstoves in Haryana, India, Atmos. Chem. Phys., 18, 2461-2480, https://doi.org/10.5194/acp-18-2461-2018, 2017.

Fu, P., Kawamura, K., Chen, J., Qin, M., Ren, L., Sun, Y., Wang, Z., Barrie, L. A., Tachibana, E., Ding, A., and Yamashita, Y.: Fluorescent water-soluble organic aerosols in the High Arctic atmosphere, Sci Rep, 5, 9845, https://doi.org/10.1038/srep09845, 2015.

Gentner, D. R., Jathar, S. H., Gordon, T. D., Bahreini, R., Day, D. A., El Haddad, I., Hayes, P. L., Pieber, S. M., Platt, S. M., de Gouw, J., Goldstein, A. H., Harley, R. A., Jimenez, J. L., Prevot, A. S., and Robinson, A. L.: Review of Urban Secondary Organic Aerosol Formation from Gasoline and Diesel Motor Vehicle Emissions, Environ. Sci. Technol., 51, 1074-1093, https://doi.org/10.1021/acs.est.6b04509, 2017.

Ghidotti, M., Fabbri, D., Masek, O., Mackay, C. L., Montalti, M., and Hornung, A.: Source and

Biological Response of Biochar Organic Compounds Released into Water; Relationships with Bio-Oil Composition and Carbonization Degree, Environ. Sci. Technol., 51, 6580-6589, https://doi.org/10.1021/acs.est.7b00520, 2017.

Graber, E. R., and Rudich, Y.: Atmospheric HULIS: How humic-like are they? A comprehensive and critical review, Atmos. Chem. Phys., 6, 729-753, https://doi.org/10.5194/acp-6-729-2006, 2006.

Gu, Q., and Kenny, J. E.: Improvement of Inner Filter Effect Correction Based on Determination of Effective Geometric Parameters Using a Conventional Fluorimeter, Anal. Chem., 81, 420-426, https://doi.org/10.1021/ac801676j, 2009.

Hecobian, A., Zhang, X., Zheng, M., Frank, N., Edgerton, E. S., and Weber, R. J.: Water-Soluble Organic Aerosol material and the light-absorption characteristics of aqueous extracts measured over the Southeastern United States, Atmos. Chem. Phys., 10, 5965-5977, https://doi.org/10.5194/acp-10-5965-2010, 2010.

Jiang, B., Kuang, B. Y., Liang, Y., Zhang, J., Huang, X. H. H., Xu, C., Yu, J. Z., and Shi, Q.: Molecular composition of urban organic aerosols on clear and hazy days in Beijing: a comparative study using FT-ICR MS, Environ. Chem., 13, 888-901, https://doi.org/10.1071/en15230, 2016.

~~Kahnt, A., Behrouzi, S., Vermeylen, R., Safi Shalamzari, M., Vercauteren, J., Roekens, E., Claeys, M., and Maenhaut, W.: One-year study of nitro-organic compounds and their relation to wood burning in PM10 aerosol from a rural site in Belgium, Atmos. Environ., 81, 561-568, https://doi.org/10.1016/j.atmosenv.2013.09.041, 2013.~~

Kirchstetter, T. W., and Thatcher, T. L.: Contribution of organic carbon to wood smoke particulate matter absorption of solar radiation, Atmos. Chem. Phys., 12, 5803-5816, https://doi.org/10.5194/acp-12-6067-2012, 2012.

Koch, B., and Dittmar, T.: Koch, B. P. & Dittmar, T. From mass to structure: An aromaticity index for high-resolution mass data of natural organic matter. Rapid Commun. Mass Spectrom. 20, 926-932, Rapid Commun. Mass Spectrom., 20, 926-932, https://doi.org/10.1002/rcm.2386, 2006.

Kumar, N. K., Corbin, J. C., Bruns, E. A., Massabó, D., Slowik, J. G., Drinovec, L., Močnik, G.,

Prati, P., Vlachou, A., Baltensperger, U., Gysel, M., El-Haddad, I., and Prévôt, A. S. H.: Production of particulate brown carbon during atmospheric aging of residential wood-burning emissions, Atmos. Chem. Phys., 18, 17843-17861, https://doi.org/10.5194/acp-18-17843-2018, 2018.

Laskin, A., Laskin, J., and Nizkorodov, S. A.: Chemistry of atmospheric brown carbon, Chem. Rev., 115, 4335-4382, https://doi.org/10.1021/cr5006167, 2015.

Laskin, A., Smith, J. S., and Laskin, J.: Molecular Characterization of Nitrogen-Containing Organic Compounds in Biomass Burning Aerosols Using High-Resolution Mass Spectrometry, Environ. Sci Technol., 43, 3764-3771, https://doi.org/10.1021/es803456n, 2009.

Lee, H. J., Laskin, A., Laskin, J., and Nizkorodov, S. A.: Excitation-emission spectra and fluorescence quantum yields for fresh and aged biogenic secondary organic aerosols, Environ. Sci. Technol., 47, 5763-5770, https://doi.org/10.1021/es400644c 2013.

Li, C., He, Q., Schade, J., Passig, J., Zimmermann, R., Meidan, D., Laskin, A., and Rudich, Y.: Dynamic changes in optical and chemical properties of tar ball aerosols by atmospheric photochemical aging, Atmos. Chem. Phys., 19, 139-163, https://doi.org/10.5194/acp-19-139-2019, 2019.

Li, M., Fan, X., Zhu, M., Zou, C., Song, J., Wei, S., Jia, W., and Peng, P.: Abundances and light absorption properties of brown carbon emitted from residential coal combustion in China, Environ. Sci. Technol., 53, 595-603, https://doi.org/10.1021/acs.est.8b05630, 2018.

Lin, P., Rincon, A. G., Kalberer, M., and Yu, J. Z.: Elemental composition of HULIS in the Pearl River Delta Region, China: results inferred from positive and negative electrospray high resolution mass spectrometric data, Environ. Sci. Technol., 46, 7454-7462, https://doi.org/10.1021/es300285d, 2012a.

Lin, P., Yu, J. Z., Engling, G., and Kalberer, M.: Organosulfates in humic-like substance fraction isolated from aerosols at seven locations in East Asia: a study by ultra-high-resolution mass spectrometry, Environ. Sci. Technol., 46, 13118-13127, https://doi.org/10.1021/es303570v, 2012b.

~~Lin, P., Aiona, P. K., Li, Y., Shiraiwa, M., Laskin, J., Nizkorodov, S. A., and Laskin, A.: Molecular Characterization of Brown Carbon in Biomass Burning Aerosol Particles, Environ. Sci.~~

~~Technol., 50, 11815-11824, https://doi.org/10.1021/acs.est.6b03024, 2016.~~

Lin, P., Aiona, P. K., Li, Y., Shiraiwa, M., Laskin, J., Nizkorodov, S. A., and Laskin, A.: Molecular Characterization of Brown Carbon in Biomass Burning Aerosol Particles, Environ. Sci. Technol., 50, 11815-11824, https://doi.org/10.1021/acs.est.6b03024, 2016.

Lin, P., Fleming, L. T., Nizkorodov, S. A., Laskin, J., and Laskin, A.: Comprehensive Molecular Characterization of Atmospheric Brown Carbon by High Resolution Mass Spectrometry with Electrospray and Atmospheric Pressure Photoionization, Anal. Chem., 90, 12493-12502, https://doi.org/10.1021/acs.analchem.8b02177, 2018.

Liu, J., Bergin, M., Guo, H., King, L., Kotra, N., Edgerton, E., and Weber, R. J.: Size-resolved measurements of brown carbon in water and methanol extracts and estimates of their contribution to ambient fine-particle light absorption, Atmos. Chem. Phys., 13, 12389-12404, https://doi.org/10.5194/acp-13-12389-2013, 2013.

Liu, J., Mo, Y., Ding, P., Li, J., Shen, C., and Zhang, G.: Dual carbon isotopes ((14)C and (13)C) and optical properties of WSOC and HULIS-C during winter in Guangzhou, China, Sci. Total Environ., 633, 1571-1578, https://doi.org/10.1016/j.scitotenv.2018.03.293, 2018.

Luciani, X., Mounier, S., Redon, R., and Bois, A.: A simple correction method of inner filter effects affecting FEEM and its application to the PARAFAC decomposition, Chemom. Intell. Lab. Syst., 96, 227-238, https://doi.org/10.1016/j.chemolab.2009.02.008, 2009.

Lv, J., Zhang, S., Wang, S., Luo, L., Cao, D., and Christie, P.: Molecular-Scale Investigation with ESI-FT-ICR-MS on Fractionation of Dissolved Organic Matter Induced by Adsorption on Iron Oxyhydroxides, Environ. Sci. Technol., 50, 2328-2336, https://doi.org/10.1021/acs.est.5b04996, 2016.

Matos, J. T. V., Freire, S. M. S. C., Duarte, R. M. B. O., and Duarte, A. C.: Natural organic matter in urban aerosols: Comparison between water and alkaline soluble components using excitation–emission matrix fluorescence spectroscopy and multiway data analysis, Atmos. Environ., 102, 1-10, https://doi.org/10.1016/j.atmosenv.2014.11.042, 2015.

Mazzoleni, L. R., Ehrmann, B. M., Shen, X. H., Marshall, A. G., and Collett, J. L.: Water-Soluble Atmospheric Organic Matter in Fog: Exact Masses and Chemical Formula Identification by Ultrahigh-Resolution Fourier Transform Ion Cyclotron Resonance Mass Spectrometry, Environ. Sci. Technol., 44, 3690-3697, https://doi.org/10.1021/es903409k, 2010.

Mo, Y., Li, J., Liu, J., Zhong, G., Cheng, Z., Tian, C., Chen, Y., and Zhang, G.: The influence of solvent and pH on determination of the light absorption properties of water-soluble brown carbon, Atmos. Environ., 161, 90-98, https://doi.org/10.1016/j.atmosenv.2017.04.037, 2017.

Mo, Y., Li, J., Jiang, B., Su, T., Geng, X., Liu, J., Jiang, H., Shen, C., Ding, P., Zhong, G., Cheng, Z., Liao, Y., Tian, C., Chen, Y., and Zhang, G.: Sources, compositions, and optical properties of humic-like substances in Beijing during the 2014 APEC summit: Results from dual carbon isotope and Fourier-transform ion cyclotron resonance mass spectrometry analyses, Environ. Pollut., 239, 322-331, https://doi.org/10.1016/j.envpol.2018.04.041, 2018.

Mo, Y., Li, J., Liu, J., Zhong, G., Cheng, Z., Tian, C., Chen, Y., and Zhang, G.: The influence of solvent and pH on determination of the light absorption properties of water-soluble brown carbon, Atmos. Environ., 161, 90-98, https://doi.org/10.1016/j.atmosenv.2017.04.037, 2017.

Murphy, K. R., Butler, K. D., Spencer, R. G., Stedmon, C. A., Boehme, J. R., and Aiken, G. R.: Measurement of dissolved organic matter fluorescence in aquatic environments: an interlaboratory comparison, Environ. Sci. Technol., 44, 9405-9412, https://doi.org/10.1021/es102362t, 2010.

Murphy, K. R., Stedmon, C. A., Graeber, D., and Bro, R.: Fluorescence spectroscopy and multi-way techniques. PARAFAC, Anal. Methods, 5, 6557-6566, https://doi.org/10.1039/c3ay41160e, 2013.

Park, S., Yu, G.-H., and Lee, S.: Optical absorption characteristics of brown carbon aerosols during the KORUS-AQ campaign at an urban site, Atmos. Res., 203, 16-27, https://doi.org/10.1016/j.atmosres.2017.12.002, 2018.

Park, S. S., and Yu, J.: Chemical and light absorption properties of humic-like substances from biomass burning emissions under controlled combustion experiments, Atmos. Environ., 136, 114-122, https://doi.org/10.1016/j.atmosenv.2016.04.022, 2016.

Patriarca, C., Bergquist, J., Sjoberg, P. J. R., Tranvik, L., and Hawkes, J. A.: Online HPLC-ESI-HRMS Method for the Analysis and Comparison of Different Dissolved Organic Matter Samples, Environ. Sci. Technol., 52, 2091-2099, https://doi.org/10.1021/acs.est.7b04508, 2018.

Qin, J., Zhang, L., Zhou, X., Duan, J., Mu, S., Xiao, K., Hu, J., and Tan, J.: Fluorescence fingerprinting properties for exploring water-soluble organic compounds in PM 2.5 in an

industrial city of northwest China, Atmos. Environ., 184, 203-211, https://doi.org/10.1016/j.atmosenv.2018.04.049, 2018.

~~Riva, M., Tomaz, S., Cui, T. Q., Lin, Y. H., Perraudin, E., Gold, A., Stone, E. A., Villenave, E., and Surratt, J. D.: Evidence for an Unrecognized Secondary Anthropogenic Source of Organosulfates and Sulfonates: Gas-Phase Oxidation of Polycyclic Aromatic Hydrocarbons in the Presence of Sulfate Aerosol, Environ. Sci. Technol., 49, 6654-6664, https://doi.org/10.1021/acs.est.5b00836, 2015.~~

Saleh, R., Robinson, E. S., Tkacik, D. S., Ahern, A. T., Liu, S., Aiken, A. C., Sullivan, R. C., Presto, A. A., Dubey, M. K., Yokelson, R. J., Donahue, N. M., and Robinson, A. L.: Brownness of organics in aerosols from biomass burning linked to their black carbon content, Nat. Geosci., 7, 647-650, https://doi.org/10.1038/ngeo2220, 2014.

Schmitt-Kopplin, P., Gelencser, A., Dabek-Zlotorzynska, E., Kiss, G., Hertkorn, N., Harir, M., Hong, Y., and Gebefugi, I.: Analysis of the Unresolved Organic Fraction in Atmospheric Aerosols with Ultrahigh-Resolution Mass Spectrometry and Nuclear Magnetic Resonance Spectroscopy: Organosulfates As Photochemical Smog Constituents, Anal. Chem., 82, 8017-8026, https://doi.org/10.1021/ac101444r, 2010

Sgroi, M., Roccaro, P., Korshin, G. V., and Vagliasindi, F. G. A.: Monitoring the Behavior of Emerging Contaminants in Wastewater-Impacted Rivers Based on the Use of Fluorescence Excitation Emission Matrixes (EEM), Environ. Sci. Technol., 51, 4306-4316, https://doi.org/10.1021/acs.est.6b05785, 2017.

Shetty, N. J., Pandey, A., Baker, S., Hao, W. M., and Chakrabarty, R. K.: Measuring light absorption by freshly emitted organic aerosols: optical artifacts in traditional solvent-extraction-based methods, Atmos. Chem. Phys., 19, 8817-8830, https://doi.org/10.5194/acp-19-8817-2019, 2019.

Shimabuku, K. K., Kennedy, A. M., Mulhern, R. E., and Summers, R. S.: Evaluating Activated Carbon Adsorption of Dissolved Organic Matter and Micropollutants Using Fluorescence Spectroscopy, Environ. Sci. Technol., 51, 2676-2684, https://doi.org/10.1021/acs.est.6b04911, 2017.

Sleighter, R. L., Chen, H., Wozniak, A. S., Willoughby, A. S., Caricasole, P., and Hatcher, P. G.: Establishing a measure of reproducibility of ultrahigh-resolution mass spectra for complex

mixtures of natural organic matter, Anal. Chem., 84, 9184-9191, https://doi.org/10.1021/ac3018026, 2012.

Smith, J. S., Laskin, A., and Laskin, J.: Molecular Characterization of Biomass Burning Aerosols Using High-Resolution Mass Spectrometry, Anal. Chem., 81, 1512-1521, 2009.

Song, J., Li, M., Jiang, B., Wei, S., Fan, X., and Peng, P.: Molecular Characterization of Water-Soluble Humic like Substances in Smoke Particles Emitted from Combustion of Biomass Materials and Coal Using Ultrahigh-Resolution Electrospray Ionization Fourier Transform Ion Cyclotron Resonance Mass Spectrometry, Environ. Sci. Technol., 52, 2575-2585, https://doi.org/10.1021/acs.est.7b06126, 2018.

Song, J., Li, M., Fan, X., Zou, C., Zhu, M., Jiang, B., Yu, Z., Jia, W., Liao, Y., and Peng, P. a.: Molecular characterization of water- and methanol-soluble organic compounds emitted from residential coal combustion using ultrahigh-resolution electrospray ionization Fourier transform ion cyclotron resonance mass spectrometry, Environ. Sc.i Technol., https://doi.org/10.1021/acs.est.9b04331, 2019.

Stubbins, A., Lapierre, J. F., Berggren, M., Prairie, Y. T., Dittmar, T., and del Giorgio, P. A.: What's in an EEM? Molecular signatures associated with dissolved organic fluorescence in boreal Canada, Environ. Sci. Technol., 48, 10598-10606, https://doi.org/10.1021/es502086e, 2014.

Sun, H., Biedermann, L., and Bond, T. C.: Color of brown carbon: A model for ultraviolet and visible light absorption by organic carbon aerosol, Geophys. Res. Lett., 34, https://doi.org/10.1029/2007gl029797, 2007.

Tao, S., Lu, X., Levac, N., Bateman, A. P., Nguyen, T. B., Bones, D. L., Nizkorodov, S. A., Laskin, J., Laskin, A., and Yang, X.: Molecular Characterization of Organosulfates in Organic Aerosols from Shanghai and Los Angeles Urban Areas by Nanospray-Desorption Electrospray Ionization High-Resolution Mass Spectrometry, Environ. Sci. Technol., 48, 10993-11001, https://doi.org/10.1021/es5024674, 2014.

Tian, J., Ni, H., Cao, J., Han, Y., Wang, Q., Wang, X., Chen, L. W. A., Chow, J. C., Watson, J. G., Wei, C., Sun, J., Zhang, T., and Huang, R.: Characteristics of carbonaceous particles from residential coal combustion and agricultural biomass burning in China, Atmos. Pollut. Res., 8, 521-527, https://doi.org/10.1016/j.apr.2016.12.006, 2017.

Wang, Y., Hu, M., Lin, P., Guo, Q., Wu, Z., Li, M., Zeng, L., Song, Y., Zeng, L., Wu, Y., Guo, S.,

Huang, X., and He, L.: Molecular Characterization of Nitrogen-Containing Organic Compounds in Humic-like Substances Emitted from Straw Residue Burning, Environ. Sci. Technol., 51, 5951-5961, https://doi.org/10.1021/acs.est.7b00248, 2017.

Wells, M. J. M., Mullins, G. A., Bell, K. Y., Da Silva, A. K., and Navarrete, E. M.: Fluorescence and Quenching Assessment (EEM-PARAFAC) of de Facto Potable Reuse in the Neuse River, North Carolina, United States, Environ. Sci. Technol., 51, 13592-13602, https://doi.org/10.1021/acs.est.7b03766, 2017.

Wong, J. P. S., Nenes, A., and Weber, R. J.: Changes in Light Absorptivity of Molecular Weight Separated Brown Carbon Due to Photolytic Aging, Environ. Sci. Technol., 51, 8414-8421, https://doi.org/10.1021/acs.est.7b01739, 2017.

Wozniak, A. S., Bauer, J. E., Sleighter, R. L., Dickhut, R. M., and Hatcher, P. G.: Technical Note: Molecular characterization of aerosol-derived water soluble organic carbon using ultrahigh resolution electrospray ionization Fourier transform ion cyclotron resonance mass spectrometry, Atmos. Chem. Phys., 8, 5099-5111, https://doi.org/10.5194/acp-8-5099-2008, 2008.

Wu, G., Ram, K., Fu, P., Wang, W., Zhang, Y., Liu, X., Stone, E. A., Pradhan, B. B., Dangol, P. M., Panday, A. K., Wan, X., Bai, Z., Kang, S., Zhang, Q., and Cong, Z.: Water-Soluble Brown Carbon in Atmospheric Aerosols from Godavari (Nepal), a Regional Representative of South Asia, Environ. Sci. Technol., 53, 3471-3479, https://doi.org/10.1021/acs.est.9b00596, 2019.

Xie, M., Hays, M. D., and Holder, A. L.: Light-absorbing organic carbon from prescribed and laboratory biomass burning and gasoline vehicle emissions, Sci Rep, 7, 7318, https://doi.org/10.1038/s41598-017-06981-8, 2017.

Xie, M., Chen, X., Holder, A. L., Hays, M. D., Lewandowski, M., Offenberg, J. H., Kleindienst, T. E., Jaoui, M., and Hannigan, M. P.: Light absorption of organic carbon and its sources at a southeastern U.S. location in summer, Environ. Pollut., 244, 38-46, https://doi.org/10.1016/j.envpol.2018.09.125, 2019.

Yan, C., Zheng, M., Sullivan, A. P., Bosch, C., Desyaterik, Y., Andersson, A., Li, X., Guo, X., Zhou, T., Gustafsson, Ö., and Collett, J. L.: Chemical characteristics and light-absorbing property of water-soluble organic carbon in Beijing: Biomass burning contributions, Atmos. Environ., 121, 4-12, https://doi.org/10.1016/j.atmosenv.2015.05.005, 2015.

Yan, G., and Kim, G.: Speciation and Sources of Brown Carbon in Precipitation at Seoul, Korea: Insights from Excitation-Emission Matrix Spectroscopy and Carbon Isotopic Analysis, Environ. Sc.i Technol., 51, 11580-11587, https://doi.org/10.1021/acs.est.7b02892, 2017.

Yassine, M. M., Dabek-Zlotorzynska, E., Harir, M., and Schmitt-Kopplin, P.: Identification of weak and strong organic acids in atmospheric aerosols by capillary electrophoresis/mass spectrometry and ultra-high-resolution Fourier transform ion cyclotron resonance mass spectrometry, Anal. Chem., 84, 6586-6594, https://doi.org/10.1021/ac300798g, 2012.

Yu, H., Liang, H., Qu, F., Han, Z. S., Shao, S., Chang, H., and Li, G.: Impact of dataset diversity on accuracy and sensitivity of parallel factor analysis model of dissolved organic matter fluorescence excitation-emission matrix, Sci Rep, 5, 10207, https://doi.org/10.1038/srep10207, 2015.

Zhang, X., Lin, Y. H., Surratt, J. D., Zotter, P., Prevot, A. S. H., and Weber, R. J.: Light - absorbing soluble organic aerosol in Los Angeles and Atlanta: A contrast in secondary organic aerosol, Geophys. Res. Lett., 38, https://doi.org/10.1029/2011GL049385, 2011.

Zhang, X., Lin, Y. H., Surratt, J. D., and Weber, R. J.: Sources, composition and absorption Angstrom exponent of light-absorbing organic components in aerosol extracts from the Los Angeles Basin, Environ. Sci. Technol., 47, 3685-3693, https://doi.org/10.1021/es305047b, 2013.

Zhang, Y., Yuan, Q., Huang, D., Kong, S., Zhang, J., Wang, X., Lu, C., Shi, Z., Zhang, X., Sun, Y., Wang, Z., Shao, L., Zhu, J., and Li, W.: Direct Observations of Fine Primary Particles From Residential Coal Burning: Insights Into Their Morphology, Composition, and Hygroscopicity, Journal of Geophysical Research: Atmospheres, 123, 12,964-912,979, https://doi.org/10.1029/2018jd028988, 2018.

Zhao, Y., Hallar, A. G., and Mazzoleni, L. R.: Atmospheric organic matter in clouds: exact masses and molecular formula identification using ultrahigh-resolution FT-ICR mass spectrometry, Atmos. Chem. Phys., 13, 12343-12362, https://doi.org/10.5194/acp-13-12343-2013, 2013.

Zhu, C. S., Cao, J. J., Huang, R. J., Shen, Z. X., Wang, Q. Y., and Zhang, N. N.: Light absorption properties of brown carbon over the southeastern Tibetan Plateau, Sci. Total Environ., 625, 246-251, https://doi.org/10.1016/j.scitotenv.2017.12.183, 2018.